



RESEARCH ARTICLE

Ano1 mediates pressure-sensitive contraction frequency changes in mouse lymphatic collecting vessels

Scott D. Zawieja¹, Jorge A. Castorena¹, Peichun Gui¹, Min Li¹, Simon A. Bulley², Jonathan H. Jaggar² , Jason R. Rock³, and Michael J. Davis¹ 

Lymphatic collecting vessels exhibit spontaneous contractions with a pressure-dependent contraction frequency. The initiation of contraction has been proposed to be mediated by the activity of a Ca²⁺-activated Cl⁻ channel (CaCC). Here, we show that the canonical CaCC Anoctamin 1 (Ano1, TMEM16a) plays an important role in lymphatic smooth muscle pacemaking. We find that isolated murine lymphatic muscle cells express Ano1, and demonstrate functional CaCC currents that can be inhibited by the Ano1 inhibitor benzbramarone. These currents are absent in lymphatic muscle cells from Cre transgenic mouse lines targeted for Ano1 genetic deletion in smooth muscle. We additionally show that loss of functional Ano1 in murine inguinal-axillary lymphatic vessels, whether through genetic manipulation or pharmacological inhibition, results in an impairment of the pressure–frequency relationship that is attributable to a hyperpolarized resting membrane potential and a significantly depressed diastolic depolarization rate preceding each action potential. These changes are accompanied by alterations in action potential shape and duration, and a reduced duration but increased amplitude of the action potential-induced global “Ca²⁺ flashes” that precede lymphatic contractions. These findings suggest that an excitatory Cl⁻ current provided by Ano1 is critical for mediating the pressure-sensitive contractile response and is a major component of the murine lymphatic action potential.

Introduction

The lymphatic system returns fluid and macromolecules from the interstitial space back to the blood circulation against a net hydrostatic pressure gradient. This is achieved through a combination of extrinsic forces such as tissue compression (i.e., skeletal or smooth muscle contractions) and the intrinsic lymphatic pump generated by the active contractions of the lymphatic collecting vessels (Zawieja, 2009; Zawieja et al., 2017). Spontaneous contractile activity is characterized by the rhythmic, entrained, and rapid contractions of the lymphatic muscle layer, with shortening velocities that approach those of striated muscle (Zhang et al., 2013). Lymphatic contractile activity is impaired in lymphedema patients (Olszewski, 2002), in which peripheral lymphatic vessels display weak and/or irregular contractions. Our understanding of the molecular and ionic mechanisms underlying the initiation and regulation of spontaneous lymphatic contractions remains limited, precluding the use of pharmaceutical therapy to target the dysfunctional lymphatic pump.

Similar to arteries and arterioles, lymphatic collecting vessels integrate physical and biochemical stimuli (Zawieja, 2009), such

as pressure and vasoactive agents (Davis et al., 2008, 2009), to regulate their contractile activity. Lymphatic collecting vessels are highly sensitive to transmural pressure (Gashev et al., 2004; Zawieja, 2009) such that contraction frequency can increase 10-fold in response to less than a 10-cm H₂O change in transluminal pressure (Scallan and Davis, 2013). The mechanism underlying this pressure-dependent phenomenon is likely electrical in nature as lymphatic contractions are driven by action potentials that trigger Ca²⁺ influx through voltage-gated L-type Ca²⁺ channels (LTCCs; Lee et al., 2014; Zawieja et al., 2018). This pressure-dependent contraction frequency suggests a stretch-sensitive mechanism that increases the rate at which an action potential is initiated; however, this process has not been fully defined. The current paradigm regarding the initiation of lymphatic contraction is based on membrane potential (V_m) recordings performed primarily in guinea pig and sheep (Van Helden, 1993; Toland et al., 2000; von der Weid et al., 2001), and posits a role for the summation of stochastic, 1–2 mV spontaneous transient depolarizations, derived from an

¹Department of Medical Pharmacology and Physiology, University of Missouri, Columbia, MO; ²Department of Physiology, University of Tennessee Health Science Center, Memphis, TN; ³Department of Medicine, Boston University School of Medicine, Boston, MA.

Correspondence to Michael J. Davis: davismj@health.missouri.edu.

© 2019 Zawieja et al. This article is distributed under the terms of an Attribution–Noncommercial–Share Alike–No Mirror Sites license for the first six months after the publication date (see <http://www.rupress.org/terms/>). After six months it is available under a Creative Commons License (Attribution–Noncommercial–Share Alike 4.0 International license, as described at <https://creativecommons.org/licenses/by-nc-sa/4.0/>).

undefined calcium activated chloride channel (CaCC), to reach a critical threshold to fire an action potential (Van Helden, 1993; von der Weid et al., 2008). In contrast to the hypothesis in which spontaneous transient depolarizations are central, recent V_m recordings from lymphatic collecting vessels in rat (von der Weid et al., 2014), sheep (Beckett et al., 2007), and mice (Zawieja et al., 2018) have instead revealed a near-linear diastolic depolarization that drives action potential generation. Regardless of the mechanism, spontaneous transient depolarization summation or linear diastolic depolarization, these initiation sequences may share a similar ionic basis involving a CaCC current (I_{ClCa}) as the rate-limiting step in regulating lymphatic contraction frequency (Van Helden, 1993; Hollywood et al., 1997; McCloskey et al., 1999; Toland et al., 2000; Beckett et al., 2007; von der Weid et al., 2008; Mohanakumar et al., 2018). However, the identity of the CaCC is unknown.

Anoctamin 1 (Ano1) has been identified as the canonical CaCC in other tissues (Caputo et al., 2008; Schroeder et al., 2008; Yang et al., 2008) and has been linked to both resting V_m and vessel tone (Bulley et al., 2012) in the blood vascular system. We tested the hypothesis that Ano1 is critical to pressure-sensitive contraction frequency of the peripheral murine internodal axillary lymphatic collecting vessel (IALV), using both molecular and functional techniques with a combination of inducible or constitutive smooth muscle-targeted Ano1 knockouts (KOs) and pharmaceutical inhibition with benzbromarone. We used sharp electrode recordings to determine the role of Ano1 in the excitability of murine lymphatic smooth muscle and its contribution to the lymphatic muscle action potential. Additionally, we expressed the genetically encoded Ca^{2+} indicator GCaMP6f in lymphatic smooth muscle to test if Ano1 alters the Ca^{2+} influx through voltage-dependent Ca^{2+} channels during the lymphatic action potential. The results reveal a critical role for Ano1 in the linear diastolic depolarization phase that regulates lymphatic pacemaking. These findings shed light on the ionic basis for pressure-dependent contraction frequency and auto-rhythmicity of lymphatic muscle.

Materials and methods

Mice

WT male mice (15–35 g) on the C57BL/6J background, ROSA26 mT/mG fluorescent Cre recombinase activity reporter mice (Muzumdar et al., 2007; strain 007676), the constitutively expressed smMHC^{Cre/eGFP} (Xin et al., 2002; strain 007742), and the genetically encoded Ca^{2+} sensor GCaMP6f (Chen et al., 2013; strain 028865) were purchased from The Jackson Laboratory. The y chromosome-linked tamoxifen inducible SMMHC-CreER^{T2} mice (Wirth et al., 2008) were a gift from S. Offermanns, Max-Planck-Institut für Herz- und Lungendforschung, Bad Nauheim, Germany. c-KitCreER^{T2} mice (Heger et al., 2014) were provided by D. Saur, Technical University of Munich, Munich, Germany. An Ano1 floxed mouse was generated at the University of Tennessee, Knoxville, TN, by Jonathan H. Jaggard, and was bred to SMMHC-CreER^{T2} mice, c-KitCreER^{T2} mice, and smMHC^{Cre/eGFP} mice to generate the following genotypes: SMMHC-CreER^{T2}; Ano1fl/fl, c-KitCreER^{T2}; Ano1fl/fl, and smMHC^{Cre/eGFP}; Ano1fl/fl.

Upon induction of the Cre with tamoxifen injections, we refer respectively to these mice as SMMHC-CreER^{T2}-Ano1KO, c-KitCreER^{T2}-Ano1KO, and smMHC^{Cre/eGFP}-Ano1KO mice. Mice harboring GCaMP6f were also bred with SMMHC-CreER^{T2}; Ano1fl/fl mice to generate the SMMHC-CreER^{T2}-GCaMP6f and SMMHC-CreER^{T2}-GCaMP6f-Ano1KO mice. In addition to these models, an Ano1-GFP reporter mouse, a doxycycline-inducible SMARTTa-tetOCre mouse, and a genetically distinct Ano1 floxed mouse generated at the University of California, San Francisco, San Francisco, CA, (Schreiber et al., 2015) were provided by Jason Rock (Boston University, Boston, MA). The doxycycline-induced SMARTTa-tetOCre; Ano1fl/fl mice are herein referred to as SMARTTa-tetOCre-Ano1KO. We collectively refer to the combination of SMMHC-CreER^{T2}-Ano1KO, smMHC^{Cre/eGFP}-Ano1KO, and SMARTTa-tetOCre-Ano1KO mice as Ano1^{smKO} in passing. Genomic DNA was extracted from tail clips using the HotSHOT method (Truett et al., 2000). Genotypes were determined by PCR with PCR Super Master Polymerase Mix (B46019; Bimake) according to the provider's instructions. All animal protocols were approved by the University of Missouri Animal Care and Use Committee and conformed to the US Public Health Service policy, 1996, for the humane care and use of laboratory animals.

IALV isolation

IALVs and popliteal lymphatic vessels were isolated as previously described (Castorena-Gonzalez et al., 2018; Zawieja et al., 2018). In brief, mice were anaesthetized with pentobarbital sodium (60 mg/kg intraperitoneal (i.p.); Nembutal) and placed on a heating pad. The IALV was isolated by a midline dorsal incision and retraction of the dorsal skin that revealed the thoracoepigastric vein and the IALV running caudally along the skin connecting the inguinal and axillary lymph nodes. The perivascular adipose and connective tissue containing the IALV were excised from the retracted skin, and the mouse was euthanized via KCl overdose. After removal, the dissected tissue was pinned to a Sylgard dish in warmed Krebs buffer, and the IALV was carefully cleaned using fine forceps and microscissors. In some protocols, the entire length(s) of the IALV(s) from the conjoined inguinal and axillary nodes from either one or both sides of the mouse was/were collected for RNA purification, protein collection, immunofluorescence, and smooth muscle cell dispersion/isolation. Half lymphangion sections (i.e., containing one lymphatic valve) were used for contractile myograph, sharp electrode impalements, and Ca^{2+} imaging experiments. Popliteal vessels were isolated as previously described (Scallan and Davis, 2013).

Cre induction protocols

SMARTTa-tetOCre-Ano1KO mice were induced by five consecutive daily i.p. injections of 2 mg of doxycycline (4 mg/ml; sterile saline). SMMHC-CreER^{T2} Ano1KO, c-KitCreER^{T2} Ano1KO, and Ano1fl/fl control mice were induced by five consecutive i.p. injections of 1 mg tamoxifen (10 mg/ml; safflower oil). For some experiments, SMMHC-CreER^{T2}-GCaMP6f and SMMHC-CreER^{T2}-GCaMP6f-Ano1KO mice were induced

through feeding tamoxifen-infused rodent chow (500 mg/kg; TD130857; Envigo) over a 1-wk period. Mice were given a 2-wk recovery period following the last day of injection or feeding to clear the tamoxifen.

Determination of recombination in IALVs

Initially, we bred each inducible Cre line to the fluorescent reporter ROSA26mT/mG, in which Cre recombinase activity switches the expression of td-tomato to GFP, to determine the fidelity and efficacy of the recombinase activity in the lymphatic collecting vessel. SMMHC-CreER^{T2};ROSA26mT/mG, c-KitCreER^{T2};ROSA26mT/mG, and SMArTTa-tetOCre;ROSA26 mT/mG mice were used to identify the cell populations with Cre activity driven by the induction protocol, and to assess recombination efficiency within the lymphatic muscle layer. IALVs were isolated for confocal imaging and immunofluorescence, and recombination efficiency was determined by the percentage of double-positive GFP and smooth muscle actin (SMA) cells. Additionally, for c-KitCreER^{T2};ROSA26mT/mG mice, small sections of the jejunum (5 mm) were excised and rinsed of their luminal contents using cold Ca²⁺-free Krebs buffer to prevent tissue movement. The section of intestine was cut open and pinned down onto a 35-mm dish coated in Sylgard and maintained in cold Ca²⁺-free Krebs buffer. The mucosa and sub-mucosa layers were then carefully dissected away. The remaining tissue was imaged using a fluorescence microscope (Zeiss Axiozoom.v16) at 112× to reveal the GFP⁺ interstitial cells of Cajal network.

Lymphatic muscle cell (LMC) dissociation and collection for patch clamp

LMCs were collected by enzymatic dissociation of 1–2 IALV segments. The dissected IALVs were cleaned in Krebs buffer: 146.9 NaCl, 4.7 KCl, 2 CaCl₂ • 2H₂O, 1.2 MgSO₄, 1.2 NaH₂PO₄ • H₂O, 3 NaHCO₃, 1.5 NaHEPES, and 5 d-glucose, pH 7.4, at 37°C. Cleaned IALV segments were transferred to a 1-ml tube of low-Ca²⁺ PSS containing (in mM) 137 NaCl, 5.0 KCl, 0.1 CaCl₂, 1.0 MgCl₂, 10 HEPES, 10 glucose, and 1 mg/ml BSA at room temperature for 10 min. The solution was decanted and replaced with a similar solution containing 26 U/ml papain (Sigma-Aldrich) and 1 mg/ml dithioerythritol. The IALVs were incubated for 30 min at 37°C with occasional agitation, then transferred to a new tube containing low-Ca²⁺ physiological saline solution (PSS) containing 1.95 collagenase H (U/ml; C8051; Sigma-Aldrich) and 1.8 mg/ml collagenase F (C7926; Sigma-Aldrich), and incubated for 3 to ~5 min at 37°C. After further digestion, the remaining fragments were rinsed two or three times with low Ca²⁺ PSS without BSA and gently triturated using a fire-polished Pasteur pipette to release single cells. Isolated LMCs were stored in ice-cold isolation medium until use. Once they settled on the bottom of the chamber, LMCs were identified by their spindle-like morphology and used for whole-cell patch clamping. In some cases, LMCs were collected via micropipette for reverse transcription (RT)-PCR analysis. We also used IALVs dissected from induced SMMHC-CreER^{T2}-ROSA26mT/mG mice for fluorescence-activated cell sorting of LMCs. The above digestion protocol was modified slightly by the addition of 100 µl of 10 mg/ml elastase (LS00635;

Worthington) to the collagenase H and F cocktail. The digested vessel was then spun down at 1,000 rpm for 4 min and rinsed with low-Ca²⁺ PSS. This washing process was repeated two more times before titration. The vessel cell suspension was then passed through a Falcon cap strainer (80 µm) and re-suspended in low-Ca²⁺ PSS for sorting. Sorted GFP⁺ LMCs cells were collected in RNA isolation buffer and immediately processed for RNA purification.

RT-PCR

Total RNA was extracted from dissected and cleaned IALVs, and flash-frozen whole mouse brain or whole kidney (positive controls), using the Arcturus PicoPure RNA isolation kit (Thermo Fisher Scientific) following the manufacturer's instructions. On-column deoxyribonuclease digestion (QIAGEN) was performed to eliminate contamination of the samples from genomic DNA. Complementary DNA (cDNA) synthesis was performed with the SuperScript III First-Strand Synthesis System (Thermo Fisher Scientific) using oligonucleotide (dT) and random hexamer priming following the manufacturer's protocol. PCR was performed in a reaction mixture containing first-strand cDNA as the template, 2 mM MgCl₂, 0.25 µM primers, 0.2 mM deoxynucleotide triphosphates, and GoTaq Flexi DNA polymerase (Promega). The PCR program comprised an initial denaturation step at 95°C for 4 min, followed by 35 repetitions of the following cycle: denaturation (94°C, 30 s), annealing (30 s), and extension (72°C, 30 s). This was followed by a final elongation step for 5 min at 72°C. PCR amplification products were separated on a 2% agarose gel by electrophoresis, stained with SYBR-Safe (Thermo Fisher Scientific), and visualized by UV transillumination. All primers were designed to amplify an intron-spanning region. Our designed endpoint RT-PCR primer sequences and the quantitative PCR (qPCR) primers and probes purchased from IDT are listed in Table 1.

Western blot analysis

IALVs were dissected as described above, IALVs were pooled from two animals to generate one sample, and sections of brain and lung tissue were taken for positive controls. For protein extraction, IALVs were homogenized using a precooled pestle and mortar in 20 µl cold radioimmunoprecipitation assay buffer (RIPA) buffer plus 1% protease inhibitor cocktail (Sigma-Aldrich). The homogenate was incubated on ice for 30 min, and then sonicated for 1 min before removal of cellular debris with centrifugation at 8,000 g for 5 min at 4°C. The bicinchoninic acid (BCA) protein assay kit (Thermo Fisher Scientific) was used to determine protein concentration. Approximately 10–20 µg of total protein was incubated for 5 min at 90°C with freshly prepared 2× Laemmli buffer containing β-mercaptoethanol (5% vol/vol) and then loaded onto 4–20% TGX Precast Gels (Bio-Rad). Separated proteins were then transferred onto a polyvinylidene difluoride membrane (Bio-Rad) overnight at 4°C. The membranes were first probed with Rabbit Anol polyclonal antibody (1:1,000 dilution; 53212; Abcam) followed by anti-rabbit horseradish peroxidase-conjugated secondary antibody (1: 8,000 dilution; 65-6120; Thermo Fisher Scientific). Bound antibodies for Anol were detected using SuperSignal West Femto ECL

Table 1. Primers used for qPCR and RT-PCR

qPCR primers				
Gene	Accession no.	Catalog Number	Description	
Ano1	NM_178642	IDT Mm.PT.58.12522115	Mouse Ano1 TaqMan probe IDT	
SMA	NM_007392	IDT Mm.PT.58.16320644	Mouse α -actin TaqMan probe IDT	
β -Actin	NM_007393	IDT Mm.PT.58.33257376.gs	Mouse Actb TaqMan probe IDT	
End point RT-PCR				
Gene	Accession no.	Strand	Sequence / Catalog Number	Amplicon (bp)
Ano1	NM_178642	F	5'-GGCATTGTGTCATTGTCTTCCAG-3'	141
		R	5'-TCCTCACGCATAAACAGCTC-3'	
TMEM16B	NM_153589	F	5'-TTTATGATTGCCCTGACGTTCTC-3'	141
		R	5'-GAGGTTGATGATGACTGCTGTT-3'	
Bestrophin 1	NM_011913	F	5'-ACACAACACATTCTGGGTGC-3'	123
		R	5'-CGCAAAGTACACACCTCATTCA-3'	
Bestrophin 2	NM_001130194.1	F	5'-TCCAGGGCTCCACCTTTGATATAG-3'	101
		R	5'-AAAGTCCCGTGAACCTCTCC-3'	
CLCA1	NM_017474	F	5'-GAAATCCCCAGCCCTGTAACAG-3'	144
		R	5'-TCGGCACCTGCTCCGTTATC-3'	
CLCA3A1	NM_009899	F	5'-GTGGACCAGCCTTTCTACATGTCTAG-3'	114
		R	5'-TGTGACACAGTTGCCTCTCTCA-3'	
NKCC1 (<i>Slc12a2</i>)	NM_009194	F	IDT Mm.PT.58.32659494	131
		R		
NKCC2 (<i>Slc12a1</i>)	NM_001079690	F	IDT Mm.PT.58.29984258	118
		R		

List of all the primer sequences, their corresponding gene accession no. used for their design, and the predicted amplicon size. F, forward; R, reverse.

Chemiluminescent Substrate (Thermo Fisher Scientific), and chemiluminescence signals were detected with a ChemiDoc XRS + System (Bio-Rad).

Immunofluorescence via confocal microscopy

IALVs were cannulated, pressurized, and fixed with 4% paraformaldehyde for 45 min at room temperature. The IALVs were then washed with PBS and blocked overnight with 5% goat serum in PBS at 4°C. Next, the IALVs were incubated overnight in PBS with the corresponding primary antibodies: anti-SMA, 1:500 (A2547; Sigma-Aldrich), anti-GFP, 1:200 (A11122; Thermo Fisher Scientific), anti-Ano1 (SP31 ab64085; Abcam), or anti-Ano1, 1:100 (HPA032148; Sigma-Aldrich). IALVs were then washed with PBS and incubated overnight with the corresponding goat secondary antibodies (Thermo Fisher Scientific) at 1:200 or Avidin-Texas Red to stain mast cells. We reserved the Alexa Fluor 488-conjugated secondary antibodies for the corresponding anti-GFP primary antibody to prevent residual GFP fluorescence from confounding colocalization in IALVs isolated from mice with GFP expression (ROSA26mTmG and smMHC^{Cre/eGFP} mice). After a final wash, IALVs were recannulated and pressurized for imaging using an inverted Olympus IX81 microscope equipped with a Yokagawa spinning disk and Hamamatsu Orca Flash4 camera using an Olympus UPlanSApo

20× objective. Popliteal lymphatic vessels from Ano1-GFP mice were pressure fixed in a similar fashion and blocked for 3 h with 5% goat serum and stained overnight with anti-SMA conjugated to Cy3 (C6198; Sigma-Aldrich) and rabbit anti-GFP conjugated to AF488 (A-21311; Thermo Fisher Scientific). After washing, these vessels were imaged using an Olympus UApoN340 40× objective. Maximum z-stack projections were created with ImageJ from z-stacks taken at 1-micron intervals.

Patch clamp protocols

Conventional whole-cell voltage clamp was performed using single lymphatic muscle cells as determined by their morphology and/or GFP fluorescence upon dissociation. Pipettes were pulled from borosilicate glass and heat polished to 3–5 M Ω . For conventional whole-cell recording, the pipette solution contained (in mM) 126 CsCl, 10 HEPES, 10 d-glucose, 1 EGTA, 1 MgATP, 1 MgCl₂, 0.2 GTP-Na, and 40 sucrose, with pH adjusted to 7.2 using CsOH. The pipette solution also contained either 0.7 mM or 0.9 mM CaCl₂ to achieve 200 nM or 1 μ M free Ca²⁺, respectively (Thomas-Gatewood et al., 2011). The bath solution contained (in mM) 126 N-methyl-d-glutamate Cl⁻, 10 HEPES, 10 d-glucose, 2 CaCl₂, 1.2 MgCl₂, and 40 sucrose, with pH adjusted to 7.4 using HCl (Thomas-Gatewood et al., 2011), and it constantly perfused the chamber. Currents were recorded using

a patch-clamp amplifier (EPC-9; HEKA) and sampled at 20 kHz with analogue filtering at 6.67 kHz using a voltage ramp protocol from a holding potential of 0 mV and a voltage ramp from -100 mV to +80 mV over a period of 1 s. 1 μ l of 10 mM benzbramarone was added to the 1 ml bath to achieve final concentration of 10 μ M benzbramarone and ultimately allowed to wash out over a period of 5–10 min, and the ramp was repeated at each step unless the stability of the gigaseal was compromised. In some experiments, we added 1 μ l of 1 mM nifedipine for a final concentration of 1 μ M nifedipine to ensure L-type calcium activity did not confound our results. To study anion permeability, the conventional whole-cell configuration was used. Patch pipettes were initially dipped in pipette solution (in mM: 133 CsCl, 1 MgCl₂, 0.5 EGTA, and 10 HEPES) and then backfilled. The bath solution was standard Hanks' balanced salt solution (135 Cl⁻) with sodium chloride substituted with sodium glutamate or sodium iodide to obtain (in mM) 49 Cl⁻ and 86 glutamate, or 125 I and 10 Cl⁻ (Thomas-Gatewood et al., 2011). To minimize the junction potentials, the reference Ag/AgCl electrode was immersed in a pipette solution continuous with an agar bridge (2% agar). All patch clamp experiments were analyzed using Pulse (HEKA) and Igor (Wave Metrics).

Pressure control

Single IALV sections were then transferred to a 3-ml observation chamber, cannulated onto two glass micropipettes (30–80 μ m, OD), pressurized to 3 cm H₂O, and allowed to equilibrate to 37°C for 30 min. The cannulated IALV, with micropipette holders, observation chamber, and Burg-style V-track mounting system, was transferred to the stage of an inverted microscope (model IM-35; Zeiss). Polyethylene tubing was attached to each micropipette holder and connected to a valve that allowed pressure control to be switched between a manual reservoir and a servo-controlled pressure system (Davis et al., 2012). Input and output pressures were set briefly to 8 cm H₂O and the IALV lengthened to remove axial slack, which minimized lateral bowing and associated diameter-tracking artifacts at the higher pressures. A peristaltic pump maintained constant perfusion of the observation chamber with Krebs buffer at a rate of 0.5 ml/min while the IALV equilibrated at 37°C for 30–60 min with pressures set to 3 cm H₂O. Spontaneous contractions typically began within 10 min and stabilized by 30 min. A Windows-based computer was used to digitize the pressure transducer signals and video image of the IALV (at 30–40 Hz) from a firewire camera (Davis et al., 2012). A custom-written LabVIEW program (National Instruments) detected the inner diameter of the IALV from the video (Davis et al., 2011).

Isolated IALV pressure myography

To test the response of each IALV to pressure, the input and output pressures were lowered simultaneously from 3 to 2, 1, and 0.5 cm H₂O, then successively stepped to 1, 2, 3, 5, and 8 cm H₂O. Under these conditions, there was no imposed pressure gradient for forward flow. Spontaneous contractions were recorded at each pressure for ~2–3 min, and pressure was returned to 3 cm H₂O after culmination of the pressure step protocol. For pharmacological inhibition of Ano1, benzbramarone

was added from a 10 mM stock solution and mixed into the bath via pipetting to a final concentration of 7 μ M and contractions allowed to stabilize. The perfusion pump was stopped for the duration of the benzbramarone experiment (7–10 min) to prevent dilution effects and the pressure steps to 2, 3, and 5 cm H₂O were repeated. The IALV was then washed in Krebs buffer and the pressure steps repeated. To test the effects of genetic deletion of Ano1 from LMCs, control Ano1 f/fl, Ano1^{smKO}, and c-KitCreER^{T2}-Ano1KO IALVs were taken through the standard pressure step protocol. Some c-KitCreER^{T2}-Ano1KO IALVs were also exposed to benzbramarone near the end of the pressure step protocol. Each experiment culminated with a 20-min equilibration in Ca²⁺-free Krebs and taken through the pressure steps to determine the passive diameter curve.

Myograph data analysis

After an experiment, custom-written analysis programs (LabVIEW) were used to detect peak end diastolic diameters, end systolic diameters, and contraction frequency, computed on a contraction-by-contraction basis over time in the 1–5-min period of time corresponding to each pressure level. The data were used to calculate several commonly reported contraction parameters:

$$\% \text{ tone} = \left[\frac{\left(\text{Max Diameter} - \text{End Diastolic Diameter} \right)}{\text{Max Diameter}} \right] * 100, \quad (1)$$

$$\text{Amplitude} = \left(\frac{\text{End Diastolic Diameter} - \text{End Systolic Diameter}}{\text{End Systolic Diameter}} \right), \quad (2)$$

where Max Diameter represents the maximum passive diameter obtained in Ca²⁺-free Krebs solution at the same pressures at the end of the experiment.

V_m recordings and analysis

IALVs were isolated and pressurized as described above. 2 μ M wortmannin was applied to the perfusion bath for 30–60 min to inhibit myosin light chain kinase until contractions were blunted (<5 μ m contraction amplitude). Wortmannin has been consistently and routinely used to impair contractile activity without affecting the underlying electrical activity (Duffy et al., 2012). Impalements into lymphatic smooth muscle were made using intracellular microelectrodes (250–350 M Ω) filled with 1 M KCl, and V_m was sampled at 1 KHz using an SEC-05x amplifier (NPI) connected to a Grass S48 stimulator, viewed with a Tektronix TDS3052 digital oscilloscope, and recorded using a custom LabVIEW program. Thus, simultaneous recordings of diameter and V_m in pressurized and contracting IALVs were obtained. Once impaled, V_m was allowed to stabilize before action potentials and multiple contraction cycles were recorded for analysis. A lower concentration of benzbramarone was used in the V_m recording experiments (5 μ M), as the higher concentration typically used in contraction studies (7 μ M) routinely stopped all activity, which we suspected resulted from a cumulative effect of benzbramarone and wortmannin. In some cases, if an impalement was lost due either to mixing via pipetting or vessel movement during contraction or tone changes,

attempts were made to reimpale the same cell, if possible, or a second cell in the immediate vicinity. Once recordings were completed, the electrode was retracted and the recording was corrected for the offset potential. Action potentials were processed automatically using an in-house Python algorithm to determine resting V_m , diastolic depolarization, threshold V_m , spike V_m , plateau V_m , and time over threshold (Zawieja et al., 2018). For the initial linear diastolic depolarization phase of the action potential, the depolarization rate was obtained from a linear fit and expressed as mV/s. In the case of the fast-depolarization phase, the time-constant, τ (expressed in ms), from an exponential fit, $V(t) = e^{t/\tau}$, was calculated such that a low τ reflected a steeper curve. Membrane potential traces consisting of a minimum of three consecutive action potentials were analyzed under each condition, and the average value for each parameter was used to represent that for a single IALV.

Ca²⁺ imaging and analysis

SMMHC-CreER^{T2}-GCaMP6f mice were used as controls for SMMHC-CreER^{T2}-GCaMP6f-Ano1KO mice. IALVs were dissected and pressurized as described above and placed in an observation chamber on an inverted Olympus IX-80 confocal microscope. Contractions were blunted with 2 μ M wortmannin to prevent movement of the vessel out of focus in the z axis. Vessels were excited with a 488-nm laser and imaged at 20–50 frames per second using an electron multiplying charge-coupled device (EMCCD; Photometrics Cascade II 512) camera for 30–60 s. Sections on the periphery of image stacks that did not contain the vessel were used to determine background noise using the histogram function of ImageJ, which was then subtracted from the image stack. Maximum projections of the image stack were then used to create non-overlapping cell masks of three to five muscle cells per field of view of each vessel. Ca²⁺ traces for those cells contained 2–20 global Ca²⁺ flashes and were characterized for rise time, peak intensity (expressed as a baseline-referenced ratio, F/F_0), duration (in seconds), and total integrated signal (area under the curve) per Ca²⁺ flash. These parameters were averaged across three to five cells from a single vessel to represent that vessel as a singular data point.

Solutions and chemicals

Krebs buffer was composed of (in mM) 146.9 NaCl, 4.7 KCl, 2 CaCl₂•2H₂O, 1.2 MgSO₄, 1.2 NaH₂PO₄•H₂O, 3 NaHCO₃, 1.5 NaHEPES, and 5 d-glucose, pH 7.4, at 37°C. Krebs-BSA buffer was prepared with the addition of 0.5% (wt/vol) BSA. During cannulation the luminal and bath solutions contained Krebs solution with BSA, but during the experiment, the bath solution was constantly exchanged with Krebs solution without albumin. For the Ca²⁺-free Krebs solution, 3 mM EGTA replaced CaCl₂•2H₂O. A benzbramarone stock solution was prepared at 10 mM in DMSO, separated into aliquots, and stored at –20°C for up to 2 mo. Doxycycline was prepared at 4 mg/ml in sterile saline and separated into aliquots, and frozen at –20°C until use. Tamoxifen was dissolved to 10 mg/ml in a safflower oil-ethanol (95/5% vol/vol) solution with rocking agitation, separated into aliquots, and stored at –20°C. Wortmannin was dissolved in DMSO to a stock solution of 10 mM. All chemicals

were obtained from Sigma-Aldrich, with the exception of BSA (United States Biochemicals), and MgSO₄ and NaHEPES (Thermo Fisher Scientific).

Statistical tests

Contraction frequency, amplitude, and tone at each pressure during the pressure step protocol were assessed via repeated measures two-way ANOVA with Dunnett's post hoc tests. Dose-dependent inhibition to benzbramarone was performed at a single pressure (3 cm H₂O) and analyzed via repeated-measures one-way ANOVA. Patch clamp data were assessed through either a two-tailed *t* test or one-way ANOVA. V_m and Ca²⁺ recordings were assessed by two-tailed *t* test. Statistical significance was assumed at $P < 0.05$ and indicated with *. Values reported refer to means \pm SEMs, and *n* can be found in each figure legend.

Online supplemental material

Fig. S1 contains representative immunofluorescence image of a IALV stained with 4',6-diamidino-2-phenylindole, anti-Ano1, anti-SMA, and avidin. A sparse population of mast cells was observed in the adventitia of isolated IALVs as determined by avidin staining. While these mast cells were positive for Ano1, they did not account for the majority of the adventitial cells that stained strongly for Ano1.

Results

The CaCC Ano1 is expressed in mouse LMCs

We detected Ano1 transcript through conventional RT-PCR in both isolated whole IALVs and freshly collected LMCs (Fig. 1 A), but we did not observe expression of its paralog Ano2 (also with CaCC activity, known as TMEM16b; Fig. 1 B; Schroeder et al., 2008; Scudieri et al., 2012). Western blots of whole lymphatic IALV confirmed the presence of Ano1 protein in both its apparent dimeric and monomeric forms (Fig. 1 C). Immunofluorescence protocols identified the cells that expressed Ano1 and revealed a diffuse staining pattern (Fig. 1 D) within SMA-positive LMCs (Fig. 1, E and F). This was also further confirmed with anti-GFP (Fig. 1 H) and anti-SMA (Fig. 1 I) staining of the muscle layer of a popliteal vessel from an Ano1-GFP reporter mouse (Fig. 1 J). Interestingly, anti-Ano1 staining also revealed a morphologically heterogeneous population of adventitial cells that were SMA-negative (Fig. 1, F and J) but stained strongly for Ano1. A subpopulation of these adventitial cells displayed a round morphology and could be costained with avidin, consistent with previous reports that nonmucosal mast cells express Ano1 (Fig. S1; Chatterjee and Gashev, 2012).

Murine LMCs display a functional I_{ClCa}

Conventional whole-cell voltage clamp of freshly dispersed LMCs from IALV revealed a Cl[–] current with amplitude sensitive to pipette Ca²⁺ concentration (Fig. 2, A–C). Under high Ca²⁺-PSS pipette buffer conditions, the majority of LMCs demonstrated an increased Cl[–] current with a slight inward rectification profile (Fig. 2 A). The reversal potential of this current was –2.6 mV \pm 0.9 under equivalent pipette and bath Cl[–] concentrations, was

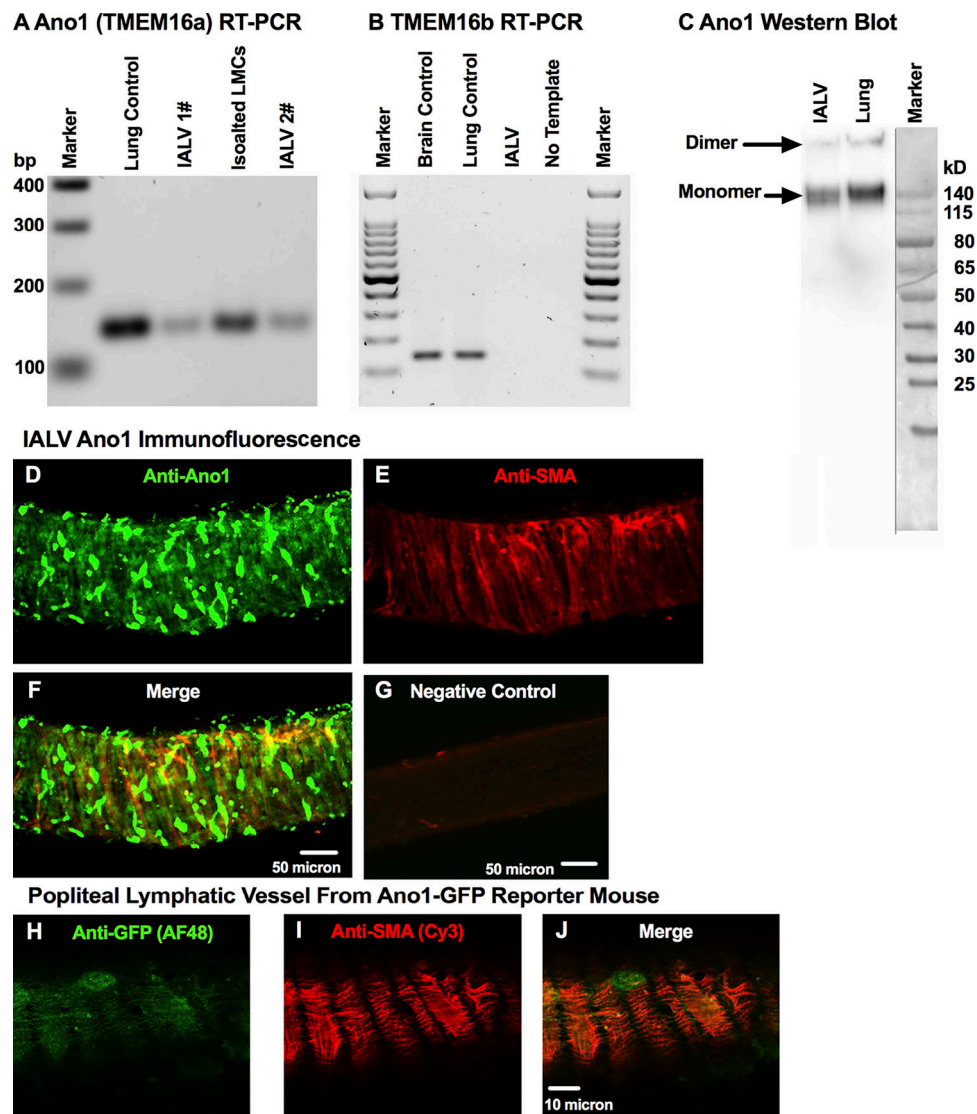


Figure 1. **Molecular evidence for Ano1 and CaCC current in LMCs.** Representative RT-PCR, resolved by agarose gel electrophoresis, for Ano1 (TMEM16a) (A) and TMEM16b (B) mRNA expression in lymphatic IALVs, LMCs, with lung and brain tissue as positive controls. (C) Western blot of collected IALVs and lung lysate with both the monomeric and dimer forms of Ano1 observed. Representative immunofluorescence maximal projection of an IALV stained anti-Ano1 (D) and with anti-SMA (E) to delineate Ano1 expression in LMCs (F, merge) at 20 \times objective magnification with the corresponding negative control (G). Representative immunofluorescence maximal projection of a popliteal lymphatic vessel isolated from an Ano1-GFP reporter mouse was stained with anti-GFP conjugated to AF488 (H) and anti-SMA conjugated to Cy3 (I) to further demonstrate LMC expression of Ano1 (J, merge).

shifted to -30.4 ± 11.5 mV when the bath solution containing 135 mM Cl^- was replaced with I^- 125 mM and 10 mM Cl^- , and shifted to 23.4 ± 7.4 mV when Cl^- was replaced with 86 mM glutamate and 38 mM Cl^- (Fig. 2, D and E). These values closely approximate the theoretical reversal potentials of -30 mV and 26 mV expected for a pure Cl^- current (Thomas-Gatewood et al., 2011). We also ruled out Ca^{2+} entry through L-type calcium channels by repeating the voltage ramp protocol in the presence 1 μM nifedipine (Fig. 2 F) and found no significant differences in the recorded currents (Fig. 2, G and H).

Ano1 has been associated with both the canonical I_{ClCa} and the bestrophin mediated cGMP-dependent I_{ClCa} observed in vascular smooth muscle (Dam et al., 2014a), and we tested whether the LMC I_{ClCa} was cGMP-dependent. RT-PCR confirmed the

expression of Bestrophin1, but not Bestrophin2, transcript in whole IALV cDNA preparations (Fig. 3 A); however, LMC Cl^- currents were not potentiated by the cGMP analogue 8-br-cGMP (300 μM) nor inhibited by ZnCl_2 (10 μM , Fig. 3, B–D) in contrast to what would be expected from bestrophin-mediated cGMP-sensitive Cl^- current. We also confirmed previous reports of messenger RNA (mRNA) expression of CLCA3A1 (Furuya et al., 2010; formerly designated mCLCA1) in the IALV extracts, likely derived from lymphatic endothelial cells, but failed to observe expression of CLCA1 (Fig. 3 A), whose orthologue in humans has been shown to modulate Ano1 activity (Sala-Rabanal et al., 2015). We also detected the expression of the $\text{Na}^+\text{K}^+\text{Cl}^-$ cotransporter (NKCC) 1 (Fig. 3 E), but not NKCC2 (Fig. 3 F), in purified IALV LMCs via RT-PCR.

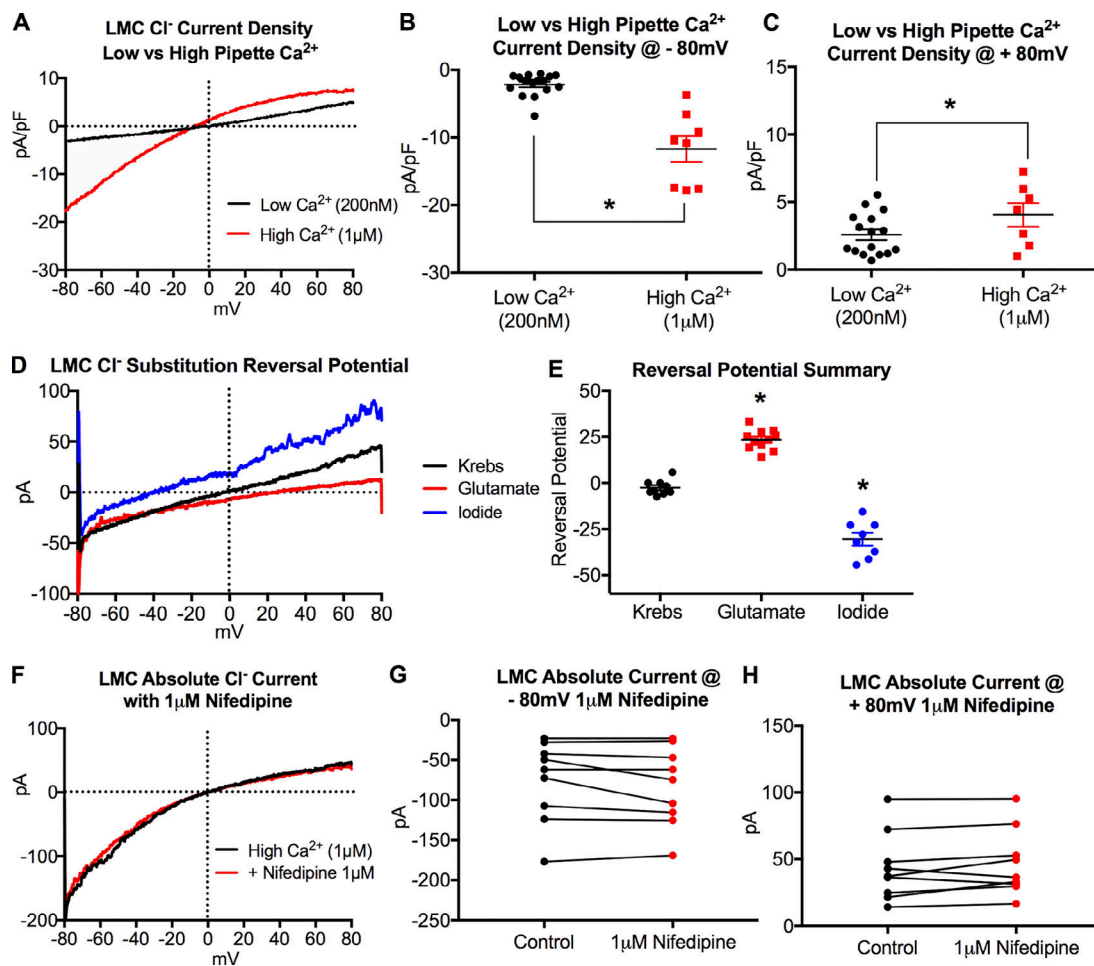


Figure 2. **IALV LMCs display a functional CaCC current.** (A) Representative recordings of whole cell patch clamp experiments designed to assess Cl^- current of freshly dissociated LMCs with either low Ca^{2+} (200 nM, black trace, $n = 16$ LMCs) or high Ca^{2+} (1 μM , red trace, $n = 8$ LMCs) in the patch pipette. Statistical analysis of current density at both -80 mV (B) and $+80$ mV (C). Representative traces showing current reversal potential with Krebs bath solution 135 mM Cl^- ($n = 9$) substituted with either glutamate (86 mM glutamate and 38 mM Cl^- , $n = 11$) or iodide (125 mM I^- and 10 mM Cl^- , $n = 8$). Representative raw traces in each buffer (D) and the summary data (E). Representative current trace in response to a voltage ramp protocol during conventional whole-cell patch clamp with or without 1 μM nifedipine present to block Ca^{2+} entry through L-type channels (F). A summary of recorded currents at -80 mV (G) and $+80$ mV (H) with or without nifedipine ($n = 8$ cells). pA, picoamperes; pF, picofarad. *, $P < 0.05$.

Ano1 is required for LMC I_{ClCa} and IALV pressure-sensitive contraction frequency

After demonstrating functional I_{ClCa} in LMCs, we used the *y* chromosome-linked, tamoxifen-inducible, smooth muscle-targeted Cre mice (SMMHC-Cre^{ERT2}) to delete *Ano1* from LMCs to specifically test the role of *Ano1* in the regulation of lymphatic pacemaking. We first tested the recombination efficiency of the SMMHC-Cre^{ERT2} in lymphatic muscle cells by crossing it to the fluorescent reporter ROSA26mT/mG and consistently observed >95% recombination of the IALV LMC population using our induction protocol (Fig. 4 A). LMCs isolated from SMMHC-Cre^{ERT2}-*Ano1*KO IALVs also had significantly reduced Cl^- current (Fig. 5 A), even with high pipette Ca^{2+} , at both positive (Fig. 5 B) and negative membrane potentials (Fig. 5 C) when compared with *Ano1*fl/fl control LMCs. At the whole vessel level, full-length IALV pairs isolated from SMMHC-Cre^{ERT2}-*Ano1*KO mice had a 60% reduction in *Ano1* mRNA compared with *Ano1*fl/fl controls as determined by qPCR (Fig. 5 D) in SMMHC-Cre^{ERT2}-*Ano1*KO

mice. Presumably the residual *Ano1* message came from endothelial cells or adventitial cells. *Ano1*fl/fl control IALVs maintained a typical contraction pattern in response to the pressure step protocol (Fig. 5 E). Strikingly, the contraction frequency of the SMMHC-Cre^{ERT2}-*Ano1*KO IALV did not change with pressure over the course of the entire pressure range (Fig. 5, F and G, i.e., pressure-dependent contraction frequency was abolished, resulting in a significantly reduced contraction frequency compared with controls at all pressures tested. In contrast, there were no significant differences in contraction amplitude (Fig. 5 H) or tone (Fig. 5 I) at any pressure between vessels from *Ano1*fl/fl control mice and SMMHC-Cre^{ERT2}-*Ano1*KO mice.

Loss of IALV pressure-dependent contraction frequency consistently observed in *Ano1*^{smKO} but not in *c-Kit*Cre^{ERT2} in *Ano1*KO

To further confirm that the lack of pressure-dependent contraction frequency was not strain- or induction protocol-dependent,

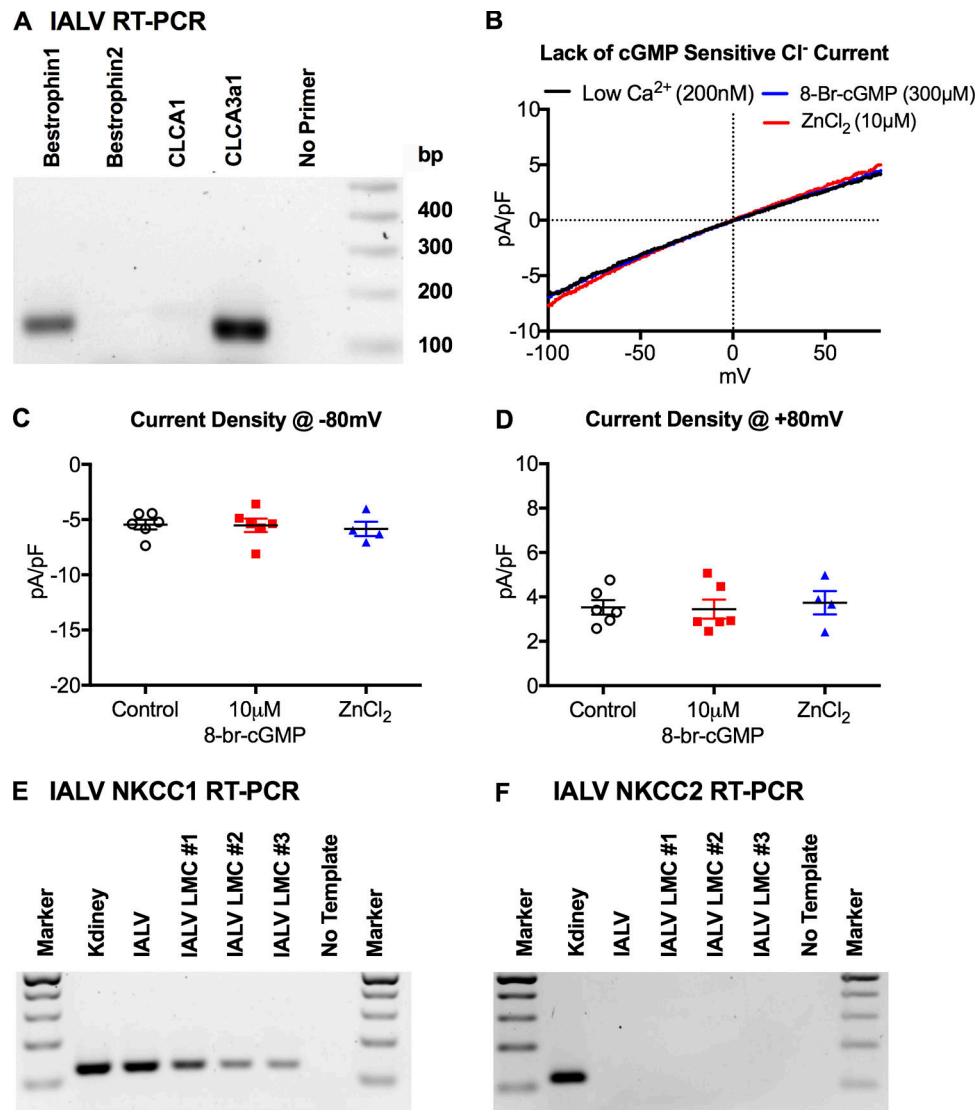


Figure 3. **The IALV LMC CaCC is not cGMP-dependent.** (A) Representative RT-PCR for bestrophin 1, bestrophin 2, CLCA1, and CLCA3 expression in IALV. (B) Representative Cl⁻ current density trace in response to a voltage ramp protocol during whole-cell conventional patch clamp of freshly dispersed IALV LMCs (n = 6), in response to stimulation with 300 nM 8-br-cGMP (n = 6), and 10 μM ZnCl₂ (n = 4). Summary of current density at -80 mV (C) and +80 mV (D). Representative RT-PCR for NKCC1 (E) and NKCC2 (F) in IALVs and LMCs purified from IALVs with kidney extract as a positive control.

we used two other distinct smooth muscle targeted Cre lines, the doxycycline-inducible SMArTTa-tetOCre and the constitutive smMHC^{Cre/eGFP}. Similar to SMMHC-CreER^{T2} IALVs, >95% recombination was achieved with the SMArTTa-tetOCre with our doxycycline induction protocol, based on the ROSA26mT/mG reporter (Fig. 4 B). The GFP fluorescence of the constitutive smMHC^{Cre/eGFP} was also used as a surrogate of recombination efficiency, with typically 80% recombination observed (Fig. 4 C). However, in the constitutive smMHC^{Cre/eGFP} mice, both the number of GFP⁺ cells and endogenous GFP⁺ fluorescence signal were quite variable from mouse to mouse in contrast to the consistent results achieved with the inducible Cre lines, suggesting that the smMHC^{Cre/eGFP} transgene may have a low expression/penetrance in LMCs. Consistent with the contraction phenotype observed in SMMHC-CreER^{T2}-Ano1KO IALVs, IALVs isolated from both the SMArTTa-tetOCre-Ano1KO and smMHC^{Cre/eGFP}-Ano1KO mice had

a significantly reduced contraction frequency that did not respond to changes in pressure. In all Ano1^{smKO} mice, contraction amplitude and tone were not significantly different from Ano1 fl/fl control vessels (Fig. 6, B and C). Lastly, Ano1 deletion did not seem to acutely affect LMC viability or turnover as the impairment in contraction frequency persisted for at least 4 mo after induction (Fig. 6 A).

In the intestinal tract, Ano1 is expressed almost exclusively within the c-Kit⁺ interstitial cells of Cajal that serve as pace-making cells and whose slow wave activity is dependent on Ano1 (Torihashi et al., 1995; Hwang et al., 2009; Malysz et al., 2017). We tested whether deletion of Ano1 from c-Kit⁺ cells in IALVs would alter lymphatic pacemaking. Using our tamoxifen induction protocol for the c-KitCreER^{T2}-ROSA26mT/mG mice, we observed recombination only in a sparse population of morphologically round cells located in the adventitia and in a minor

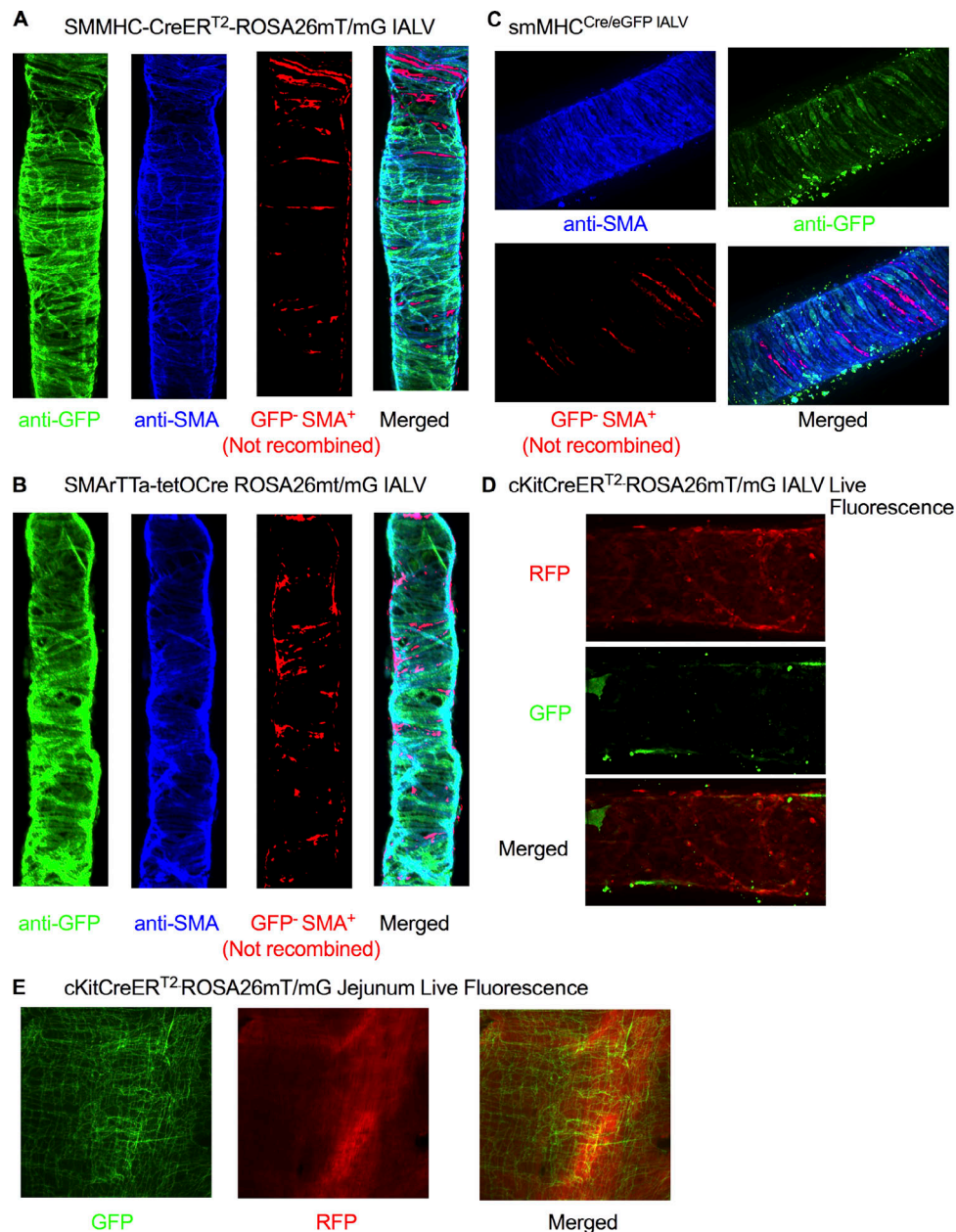


Figure 4. **Recombination efficiency of SMMHC-CreERT², SMARTTa-tetOCre, smMHC^{Cre/eGFP}, and c-KitCreERT² lines with ROSA26mT/mG.** (A) Representative immunofluorescence maximal projections of a fixed SMMHC-CreERT²-ROSA26mT/mG IALV stained for GFP and SMA to determine recombination efficiency. (B) Representative immunofluorescence maximal projections of a fixed SMARTTa-tetOCre-ROSA26mT/mG IALV stained with antibodies for GFP and SMA to determine recombination efficiency. (C) Representative immunofluorescence maximal projections of a smMHC^{Cre/eGFP} IALV fixed and stained for GFP and SMA to determine recombination efficiency. (A–C) Comparisons of cell masks for SMA and GFP to highlight cells that were SMA-positive/GFP-negative and the merged maximal projection used to assess recombination efficiency. (D) Representative immunofluorescence maximal projections of a live and pressurized (2 cm H₂O) c-KitCreERT²-ROSA26mT/mG IALV imaged for GFP (recombined cells) and td-tomato (not recombined). Images were taken at 20× objective magnification. (E) Representative immunofluorescent images of the intestine muscle layer of a c-KitCreERT²-ROSA26mT/mG induced with our tamoxifen injection protocol and acquired using a fluorescence macroscope revealed recombination of the c-Kit⁺ interstitial cells of Cajal. RFP, red fluorescent protein (tdTomato); GFP, green fluorescent protein (EGFP).

population of lymphatic endothelial cells (Fig. 4 D) despite robust labeling of interstitial cells of Cajal in the intestine of the same mice (Fig. 4 E). In contrast to the Anol^{smKO} mice, IALVs isolated from c-KitCreERT²-Anol^{KO} did not have a significantly different contraction frequency, amplitude, or tone compared with the Anol^{fl/fl} mice (Fig. 6, D–F).

Benzbromarone inhibits LMC I_{CLCa} and causes a dose-dependent inhibition of contraction frequency

Ano1 deletion from smooth muscle cells consistently resulted in a loss of LMC I_{CLCa} and abrogated the pressure-dependent contraction frequency change in murine IALVs. However, deletion of Ano1 could possibly alter the activity of other channels from a

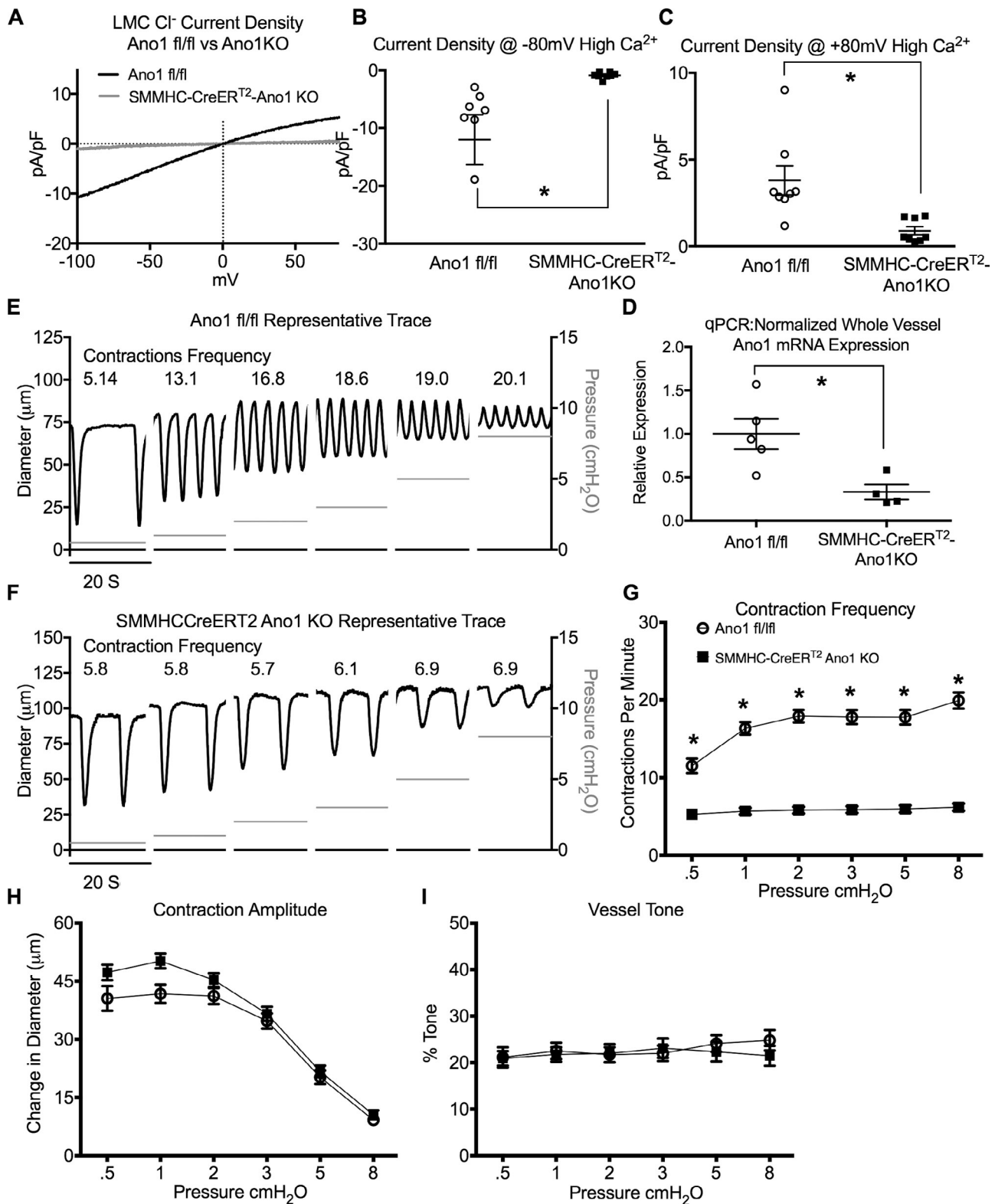


Figure 5. **Inducible deletion of Ano1 from LMCs reduces contraction frequency and abrogates pressure-dependent contraction frequency.** (A) Representative trace of Cl⁻ current density during a voltage ramp protocol using conventional whole-cell patch clamp of freshly dispersed LMCs from IALV isolated from Ano1fl/fl (*n* = 8) or SMMHC-CreERT²-Ano1KO (*n* = 8) mice (1 μM Ca²⁺ in patch pipette). Summary of current density at -80 mV (B) and +80 mV (C). (D) Normalized Ano1 expression determined by qPCR from whole IALV in Ano1fl/fl controls (*n* = 5) and SMMHC-CreERT²-Ano1KO (*n* = 4) mice. 20-s clips from a single representative inner diameter trace over the pressure step protocol for an IALV isolated from the Ano1fl/fl controls (E) and the SMMHC-CreERT²-Ano1KO mice (F). Statistical summary of contractile parameters frequency (G), amplitude (H), and tone (I) at each pressure. *, *P* < 0.05 for SMMHC-CreERT²-Ano1KO (*n* = 27) versus Ano1fl/fl controls (*n* = 22).

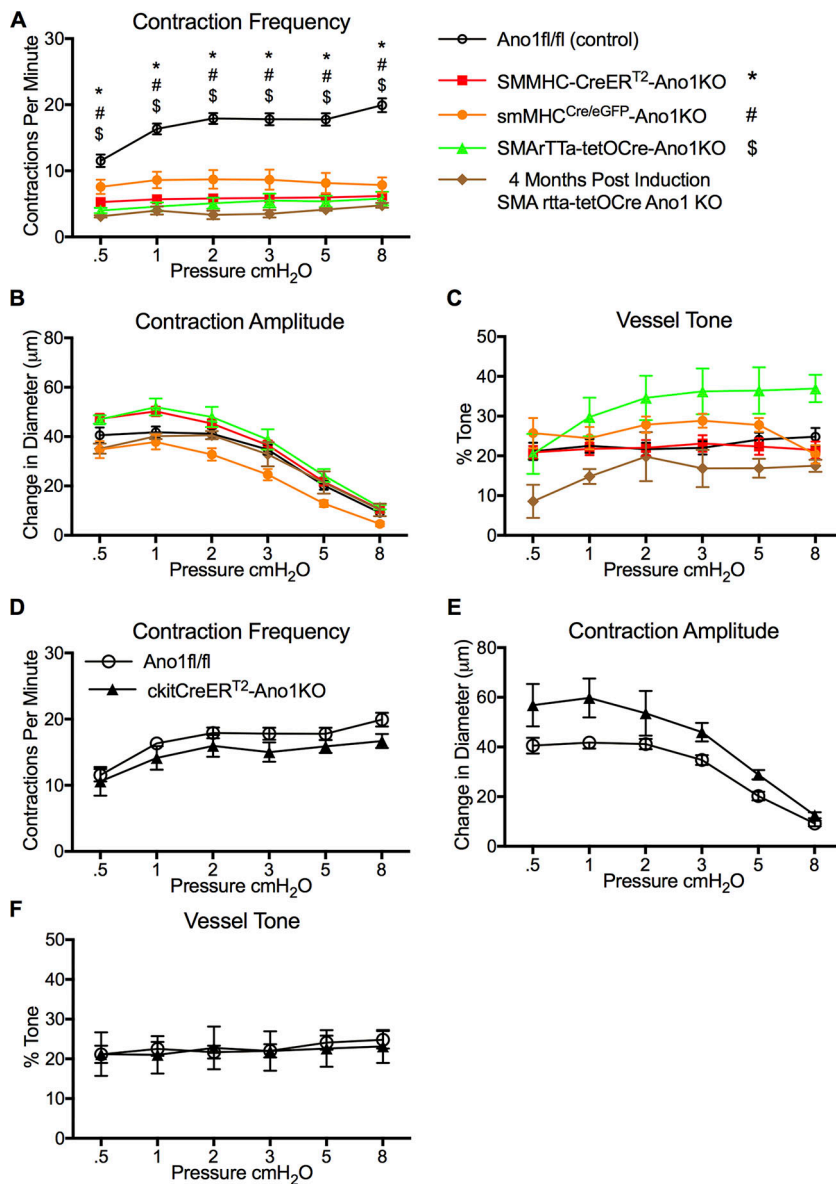


Figure 6. **IALV contractile parameters of all *Ano1^{smKO}* and *c-KitCreER^{T2} Ano1KO*.** Summary of IALV contractile parameters frequency (A), amplitude (B), and tone (C) from SMMHC-CreER^{T2}-Ano1KO, SMArTTa-tetOCre-Ano1KO, and the constitutive smMHC^{Cre/eGFP}-Ano1KO. Contractile parameters for SMArTTa-tetOCre-Ano1KO from two IALVs collected 4 mo after induction as opposed to 2 wk. *, #, and \$ denote P values < 0.05 when compared with Ano1fl/fl controls (*n* = 22) for SMMHC-CreER^{T2}-Ano1KO (*n* = 27), smMHC^{Cre/eGFP}-Ano1KO (*n* = 7), and SMArTTa-tetOCre-Ano1KO (*n* = 6), respectively. Summary of IALV contractile parameters frequency (D), amplitude (E), and tone (F) from *c-KitCreER^{T2}-Ano1KO* mice (*n* = 5) and Ano1fl/fl control mice (*n* = 22).

loss of protein-protein-dependent interactions as has been described for bestrophins (Dam et al., 2014b) and cystic fibrosis transmembrane conductance regulator (Benedetto et al., 2017) or from changes in channel expression as observed with L-type channels (Dam et al., 2014b). We used the potent Ano1 inhibitor benzbromarone (Hwang et al., 2016) to acutely test the role of Ano1-dependent I_{ClCa} of LMCs in the pressure-sensitive contraction frequency change of pressurized IALVs. Cl^- current recorded in LMCs using 200 nM Ca^{2+} pipette solution was significantly inhibited by 10 μM benzbromarone (Fig. 7 A) at both negative (Fig. 7 B) and positive voltages (Fig. 7 C) and was partially restored upon washout. As benzbromarone is a potent, but not selective, inhibitor of CaCCs (Hwang et al., 2016), we determined the benzbromarone dose-response relationship for pressurized IALVs (Fig. 7 D). Benzbromarone caused a significant, dose-dependent reduction in both contraction frequency (Fig. 7 E) and tone (Fig. 7 G), with a trend to reduce contraction amplitude at higher concentrations (Fig. 7 F),

although the latter effect was not significant. Contractions ceased at 10 μM benzbromarone in at least half of the IALVs (Fig. 7 D), precluding its use in our contractile studies at doses ≥ 10 μM, as have been used in other studies (Huang et al., 2012; Hwang et al., 2016; He et al., 2017); whether this effect was due to Ano1 inhibition or an off-target effect could not be determined.

Benzbromarone impairs pressure-dependent contraction frequency

We then assessed the IALV contractile response at pressures 2–5 cm H₂O using 7 μM benzbromarone. Representative diameter traces from a single IALV in Krebs buffer (Fig. 8 A) demonstrated a significant inhibition of contraction frequency with long pauses in diastole (Fig. 8 B) that reversed upon washout (Fig. 8 C). The effect of 7 μM benzbromarone was typically a single contraction (*, Fig. 8 B) or two successive contractions (% , Fig. 8 B) followed by long pauses; however, a new rhythm at a

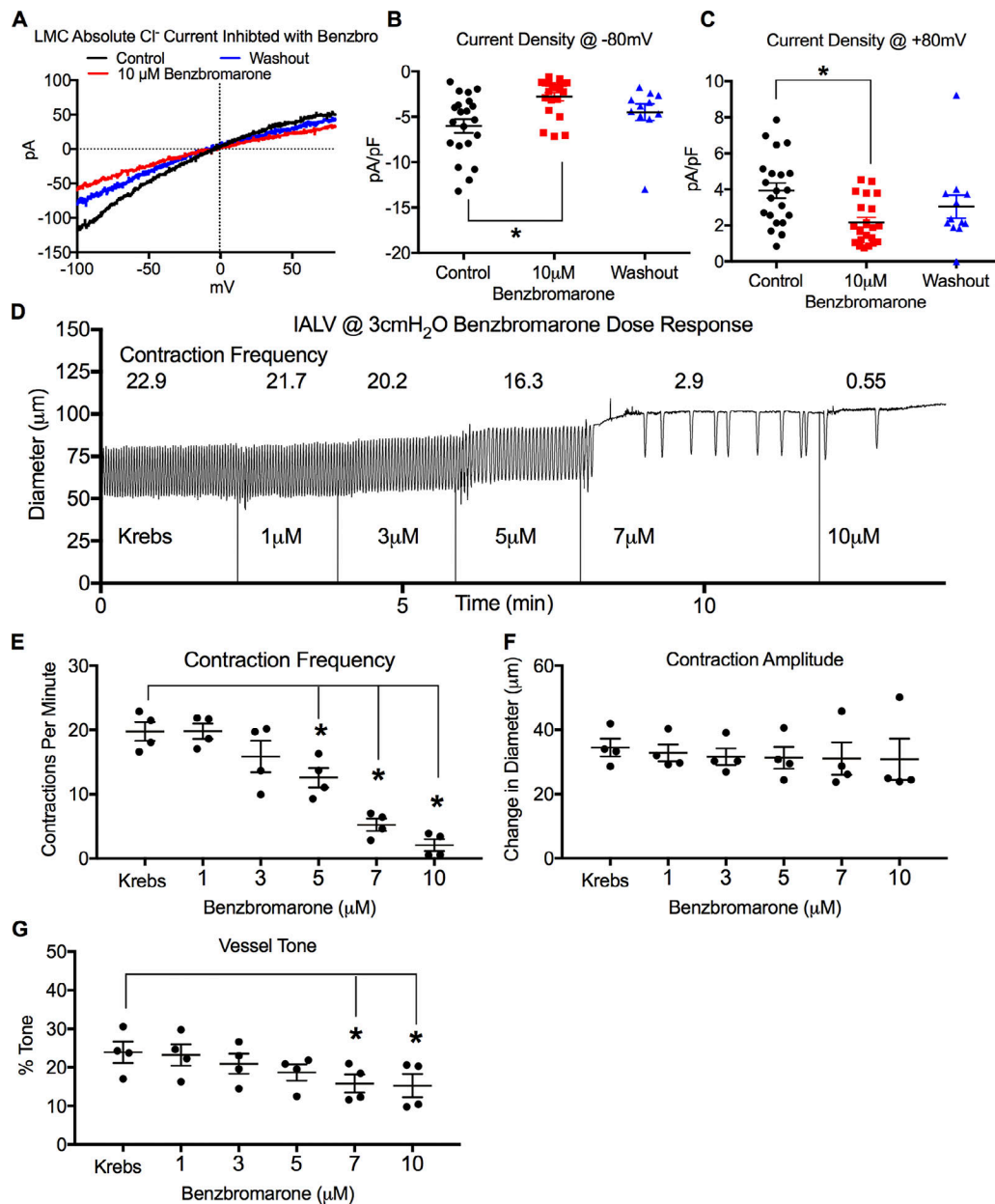


Figure 7. **Inhibition of LMC I_{ClCa} and effect of benzbromarone dose-response on IALV contractile parameters.** (A) Representative trace of absolute Cl⁻ current during a voltage ramp protocol using conventional whole-cell patch clamp of freshly dispersed LMCs in response to the Anol1 inhibitor benzbromarone and after washout (200 nM Ca²⁺ in patch pipette). Summary of current density at -80 mV (B) and +80 mV (C). $n = 23$ LMCs for control and 10 μM benzbromarone; $n = 10$ LMCs whose patch integrity persisted through washout (D). Representative inner diameter trace of a WT IALV pressurized to 3 cm H₂O in response different concentrations of benzbromarone (1, 3, 5, 7, and 10 μM). Summary of contractile parameters frequency (E), amplitude (F), and tone (G). *, $P < 0.05$ when compared with Krebs control with $n = 4$.

lower contraction frequency was maintained, as opposed to producing a stochastic contraction pattern (Fig. 8 B). As observed in the dose-response plot, 7 μM benzbromarone caused a consistent and significant reduction in basal contraction frequency (Fig. 8 D) and tone (Fig. 8 F), but not contraction amplitude (Fig. 8 E). In the presence of benzbromarone, contraction frequency did not change during pressure elevation from 2 to 3 to 5 cm H₂O. Both contraction frequency and tone recovered to their respective basal values upon benzbromarone washout. Last, 7 μM benzbromarone was able to impair the otherwise

normal contractile frequency observed in *c-KitCreER^{T2}-Ano1KO* mice (Fig. 8 G).

Ano1 is a critical determinant of contraction frequency through modulation of the membrane potential diastolic depolarization rate

As each lymphatic contraction is preceded by an action potential, we used sharp electrode membrane potential recordings to assess the role of Anol1 in setting the LMC resting membrane potential and action potential initiation in pressurized,

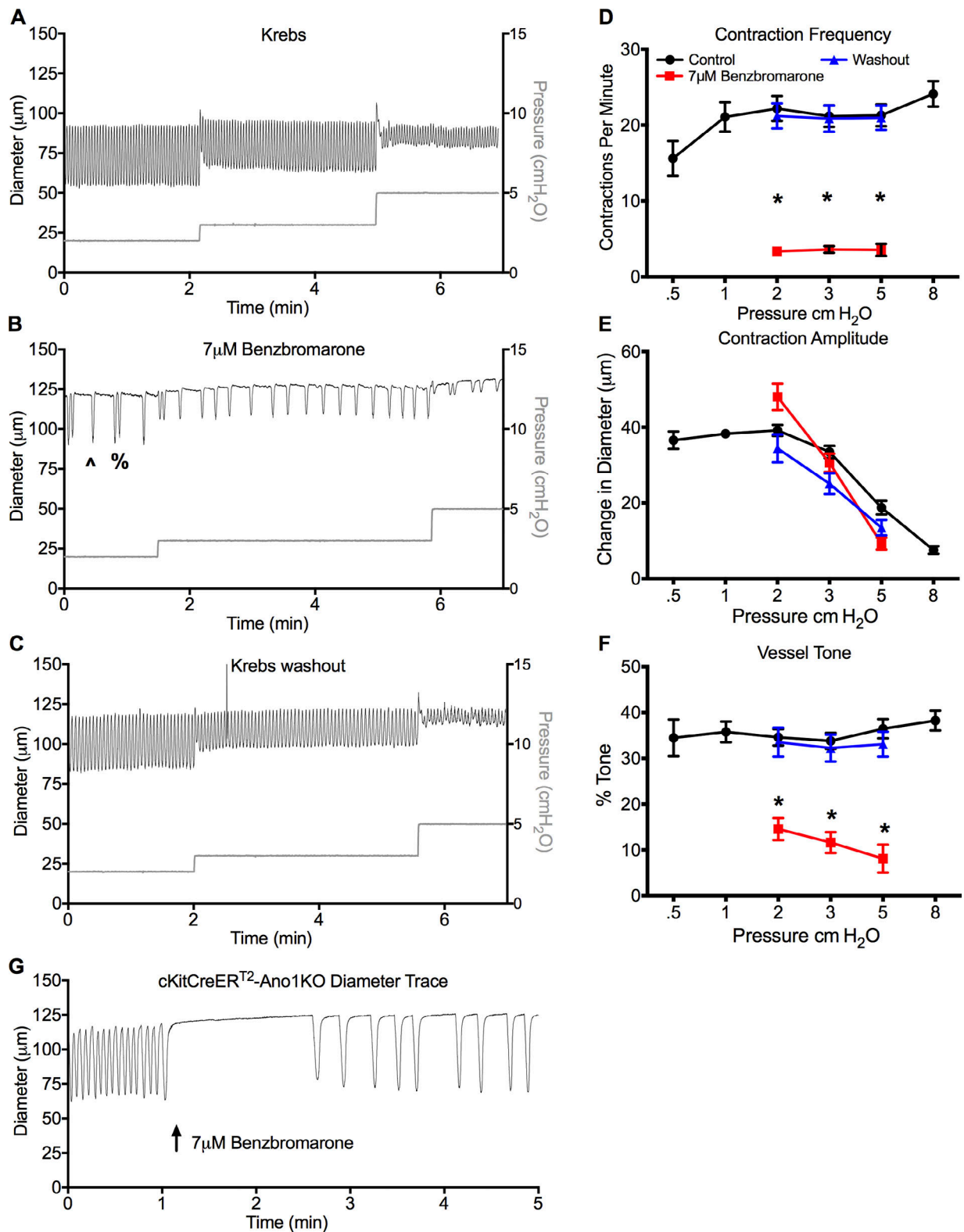


Figure 8. **Lymphatic contractile function with the Ano1 inhibitor benzbromarone.** (A–C) Representative inner diameter trace from a single IALV during the pressure step protocol (A), and at pressures 2–5 cm H₂O with 7 µM benzbromarone (B) and washout (C). (B) Both a single contraction (^) or occasionally two consecutive contractions (%) were routinely observed in 7 µM benzbromarone. Statistical comparison of summary data for the contractile parameters frequency (D), amplitude (E), and tone (F). (G) Representative trace of c-KitCreER^{T2}-Ano1KO IALV in response to 7 µM benzbromarone. *, P < 0.05 for benzbromarone versus Krebs with n = 7.

spontaneously contracting IALVs from Anol1^{fl/fl} and SMMHC-CreER^{T2}-Ano1KO mice. Membrane potential recordings of Anol1^{fl/fl} LMCs revealed action potentials at regular intervals underlying the IALV rhythmic contractile profile (Fig. 9 A). LMC membrane potential recordings in Krebs buffer (Fig. 9 A) demonstrated the typical characteristics of action potentials recorded in LMCs of pressurized IALVs (Zawieja et al., 2018): a resting membrane potential that depolarized with a linear rate until reaching a critical threshold potential at approximately -29 mV, whereupon the depolarization increased exponentially, signifying the initiation of the action potential. We often observed an action potential “spike” of ~2–5 mV in magnitude as calculated from the difference in the peak and plateau voltage. The time during which membrane potential was depolarized over the threshold potential (duration of the plateau) was ~1.2–1.3 s. No significant after-hyperpolarization was observed during the repolarization phase of the action potential (Fig. 9 A). In contrast, action potentials recorded from SMMHC-CreER^{T2}-Ano1KO mice had a distinctive change in action potential shape (Fig. 9 B) that accompanied the expected low, but still rhythmic, contraction frequency (Fig. 9 C). Resting membrane potentials were hyperpolarized in SMMHC-CreER^{T2}-Ano1KO LMCs (Fig. 9 D), and the linear diastolic depolarization rate was significantly lower (Fig. 9 E). The threshold for action potential initiation remained unchanged (Fig. 9 F); however, the rapid upstroke was significantly steeper as demonstrated by a significantly lower exponential constant “ τ ” (Fig. 9 G). This was accompanied by a significantly more depolarized peak potential, around +10 mV in this representative IALV trace (Fig. 9 B) but as high as +20 mV in other IALVs (Fig. 9 H), that did not resolve into a plateau (Fig. 9, B and I). Instead, the SMMHC-CreER^{T2}-Ano1KO action potential appeared to be a brief spike that quickly repolarized, resulting in approximately a 50% reduction in time spent over threshold potential as compared with the Anol1^{fl/fl} controls (Fig. 9 J).

The Ano1 inhibitor benzbramarone hyperpolarizes LMC resting V_m and decreases the diastolic depolarization rate to reduce contraction frequency

When membrane potential recordings were made in control vessels in Krebs buffer (Fig. 10 A), the application of 5 μ M benzbramarone significantly reduced action potential frequency (Fig. 10, B and C). Resting membrane potential was significantly hyperpolarized (Fig. 10 D) by benzbramarone, and the diastolic depolarization rate was significantly reduced (Fig. 10 E). However, the threshold potential and exponential upstroke coefficient were unchanged by benzbramarone (Fig. 10, F and G). Furthermore, benzbramarone did not significantly alter the action potential peak potential (Fig. 10 H), the plateau potential (Fig. 10 I), or the duration of the action potential as measured by time spent over the threshold potential (Fig. 10 J).

Ano1KO increases LMC action potential-driven Ca^{2+} flash peak intensity but reduces flash duration

The activation of L-type calcium channels is required for the lymphatic action potential and is involved in determining the upstroke rate constant and duration of the plateau phase

(Zawieja et al., 2018). The significant reduction in the plateau duration and the altered action potential peak potential suggest involvement of another ion, and we hypothesized that the remaining action potential profile is the result of electrogenic Ca^{2+} influx through voltage-gated Ca^{2+} channels. To test this hypothesis, we investigated the Ca^{2+} dynamics in IALVs from control SMMHC-CreER^{T2}-GCaMP6f (Fig. 11 A) and SMMHC-CreER^{T2}-GCaMP6f-Ano1KO mice (Fig. 11 B) using the genetically encoded Ca^{2+} sensor GCaMP6f. As previously described (Zawieja et al., 2018), control IALV contractions are preceded by a near-synchronous global calcium event (calcium flash), with peak intensity 3–5-fold greater than baseline, lasting ~1.5 s in each of the LMCs in the field of view; the flash corresponds with the action potential and reflects the influx of Ca^{2+} through LTCCs (Zawieja et al., 2018). During diastole, spontaneous Ca^{2+} events were observed in most LMCs, but these were not coordinated between cells, and the Ca^{2+} signal ranged 30–50% over baseline (Castorena-Gonzalez et al., 2018). In agreement with the contractile findings, the Ca^{2+} flash frequency was significantly reduced in SMMHC-CreER^{T2}-GCaMP6f-Ano1KO mice (Fig. 11 C). As expected from changes in the action potential profile, peak Ca^{2+} flash intensity F/F_0 was significantly higher (Fig. 11 D) in SMMHC-CreER^{T2}-GCaMP6f-Ano1KO IALVs, with a significantly shorter time to reach peak Ca^{2+} (Fig. 11 E), but was also significantly shorter in duration (Fig. 11 F). Despite the shorter duration, SMMHC-CreER^{T2}-GCaMP6f-Ano1KO IALVs had significantly greater Ca^{2+} entry as assessed by the area under the curve (Fig. 11 G) compared with SMMHC-CreER^{T2}-GCaMP6f control IALVs.

Discussion

The role for I_{ClCa} in the initiation of the lymphatic action potential has been suggested previously (Van Helden, 1993; Toland et al., 2000; Beckett et al., 2007; von der Weid et al., 2008), although the identity of the critical ion channel(s) in LMCs has never been determined. Here we provide definitive evidence that the CaCC Ano1 is expressed within the LMCs of murine IALVs and is necessary for the pressure-dependent change in contraction frequency observed in lymphatic collecting IALVs. Ano1 is required for LMC I_{ClCa} and is a critical determinant of the lymphatic pacemaking by providing an excitatory current that sets the slope of the diastolic depolarization, the rate-limiting step in the initiation of an action potential. Deletion of Ano1 within the LMCs resulted in an altered action potential shape that also manifested in altered Ca^{2+} dynamics despite a normal contractile amplitude. The role of Ano1 in human lymphatic contractile regulation (Mohanakumar et al., 2018) and the activity of Ano1 under pathological conditions warrant further investigation.

In the intestinal tract, Ano1 expression is almost exclusively confined to c-Kit⁺ interstitial cells of Cajal, including those located in the myenteric plexus that can be identified by their stellate morphology with widely branching processes (Gomez-Pinilla et al., 2009; Hwang et al., 2009; Drumm et al., 2017). In these pacemaker cells, Ano1 is critical to slow wave generation, effective pacemaking and coordination of intestinal smooth

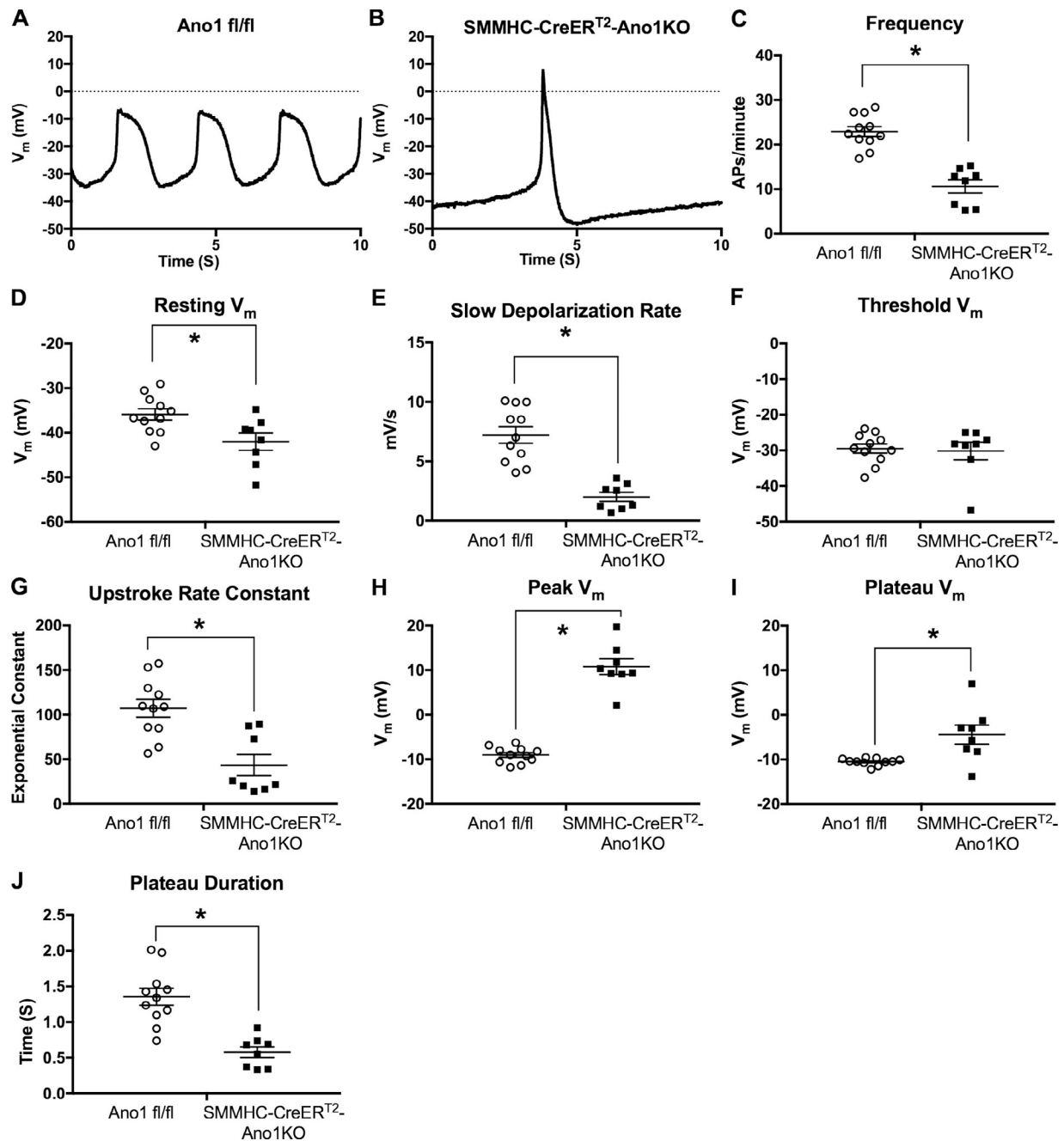


Figure 9. **Sharp electrode LMC membrane potential recordings in pressurized IALV from *Ano1fl/fl* and *SMMHC-CreERT²-Ano1KO* mice.** Representative 10-s membrane potential recording made with sharp electrode impalements of an LMCs from pressurized IALVs isolated from an *Ano1fl/fl* control mouse (A) or *SMMHC-CreERT²-Ano1KO* mouse (B). The recorded action potentials were analyzed to assess action potential frequency (C), resting membrane potential (D), the linear diastolic depolarization rate (E), the action potential initiation threshold potential (F), the steepness of the action potential upstroke (G), peak voltage achieved during the action potential (H), the plateau voltage (I), and plateau duration (J). *, $P < 0.05$ comparing *SMMHC-CreERT²-Ano1KO* ($n = 8$) versus *Ano1fl/fl* ($n = 11$).

muscle contraction (Hwang et al., 2009; Hennig et al., 2010; Malysz et al., 2017). Recently, *c-Kit*⁺ adventitial cells were reported in the human lymphatic thoracic duct and regarded as interstitial cells of Cajal-like cells based on staining with methylene blue dye, transmission electron microscopy, and immunostaining for vimentin, CD34, and *c-Kit* (Briggs Boedtkjer et al., 2013). In addition, *c-Kit*⁺ and vimentin⁺ cells have also been described in sheep mesenteric lymphatics (McCloskey

et al., 2002). However, our *c-KitCreERT²-ROSA26mT/mG* fluorescent reporter resulted in recombination of only a small population of large, round, adventitial cells (Fig. S1) on IALVs that we assume are mast cells based on their avidin⁺ staining profile, in agreement with previous reports (Chatterjee and Gashev, 2012; Hasselhof et al., 2016). Additionally, recombination occurred in a very minor population of endothelial cells. In contrast to the sparse recombination of cells in the IALV, we

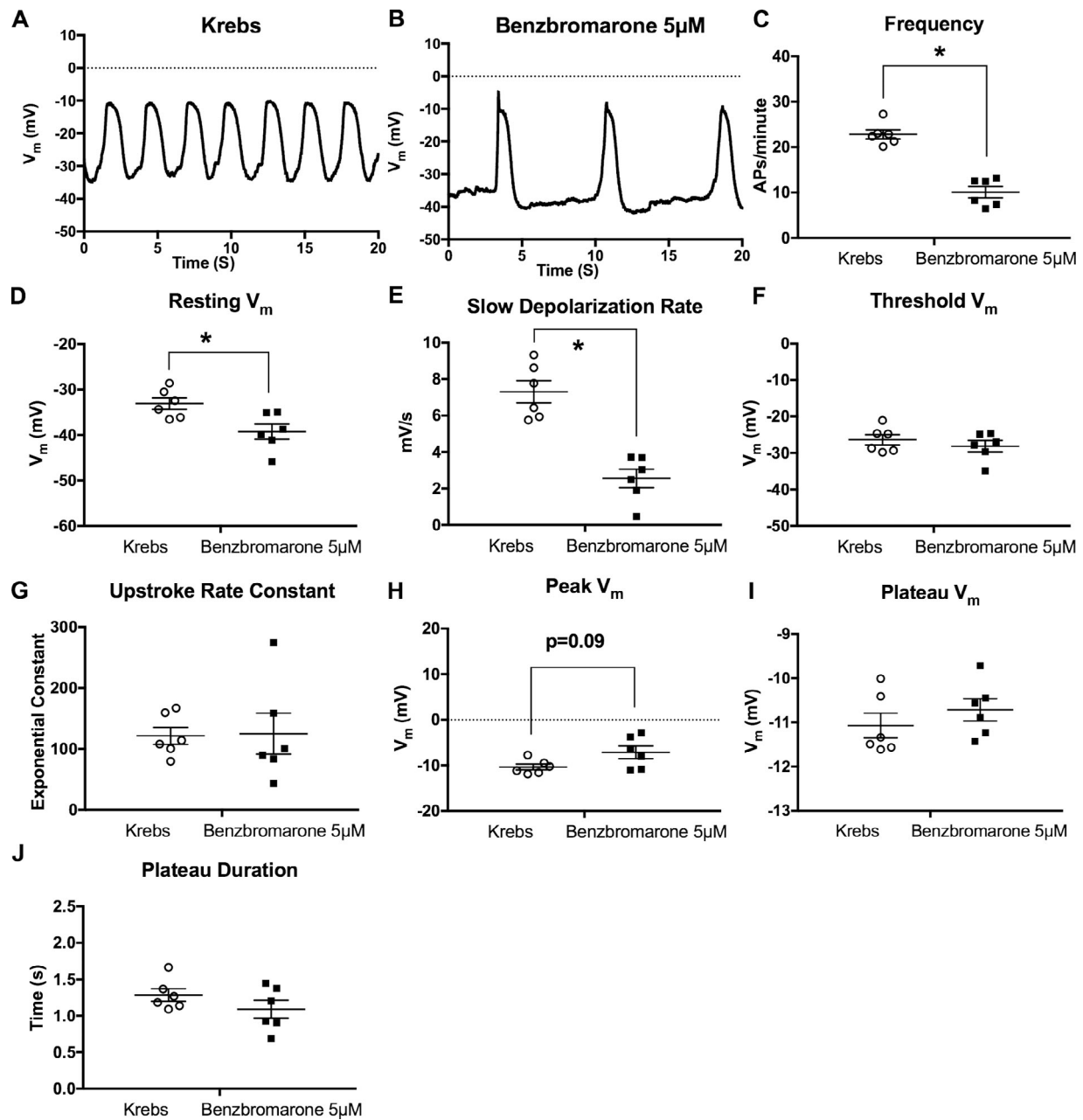


Figure 10. **Effect of the Ano1 inhibitor benzbromarone on sharp electrode LMC membrane potential of pressurized IALV.** Representative 20-s membrane potential recording made with sharp electrode impalement of a LMC from a pressurized IALV under control perfusion with Krebs solution (A) and in response to 5 μM benzbromarone (B). The recorded action potentials were analyzed to assess: action potential frequency (C), resting membrane potential (D), the linear diastolic depolarization rate (E), action potential initiation threshold potential (F), the steepness of the action potential upstroke (G), peak voltage achieved during the action potential (H), the plateau voltage (I), and plateau duration (J). *, $P < 0.05$ comparing 5 μM benzbromarone versus Krebs at $n = 6$.

could consistently observe significant recombination within the networks of interstitial cells of Cajal network of the small intestine using our induction protocol in *c-Kit*^{CreER}^{T2}-ROSA26mT/mG mice (Fig. 4 E). A recent characterization of human dermal lymphatic vessels also failed to find a significant cell *c-Kit*⁺ cell population, aside from the observation of a round, granular population of *c-Kit*⁺ mast cells, and instead revealed adventitial cells positive for PDGFR α and CD34

(Hasselhof et al., 2016). A similar PDGFR α ⁺CD34⁺ cell population may exist in the murine IALV wall and could also account for the strongly Ano1⁺ adventitial cells observed in our immunofluorescence images. The presence of a non-LMC Ano1⁺ cell population is further supported by the fact that whole-vessel Ano1 mRNA was reduced to only 40% of control levels in IALVs from SMMHCCreER^{T2}-Ano1KO mice (Fig. 5 D) despite over 95% recombination in LMCs. Research into the identity

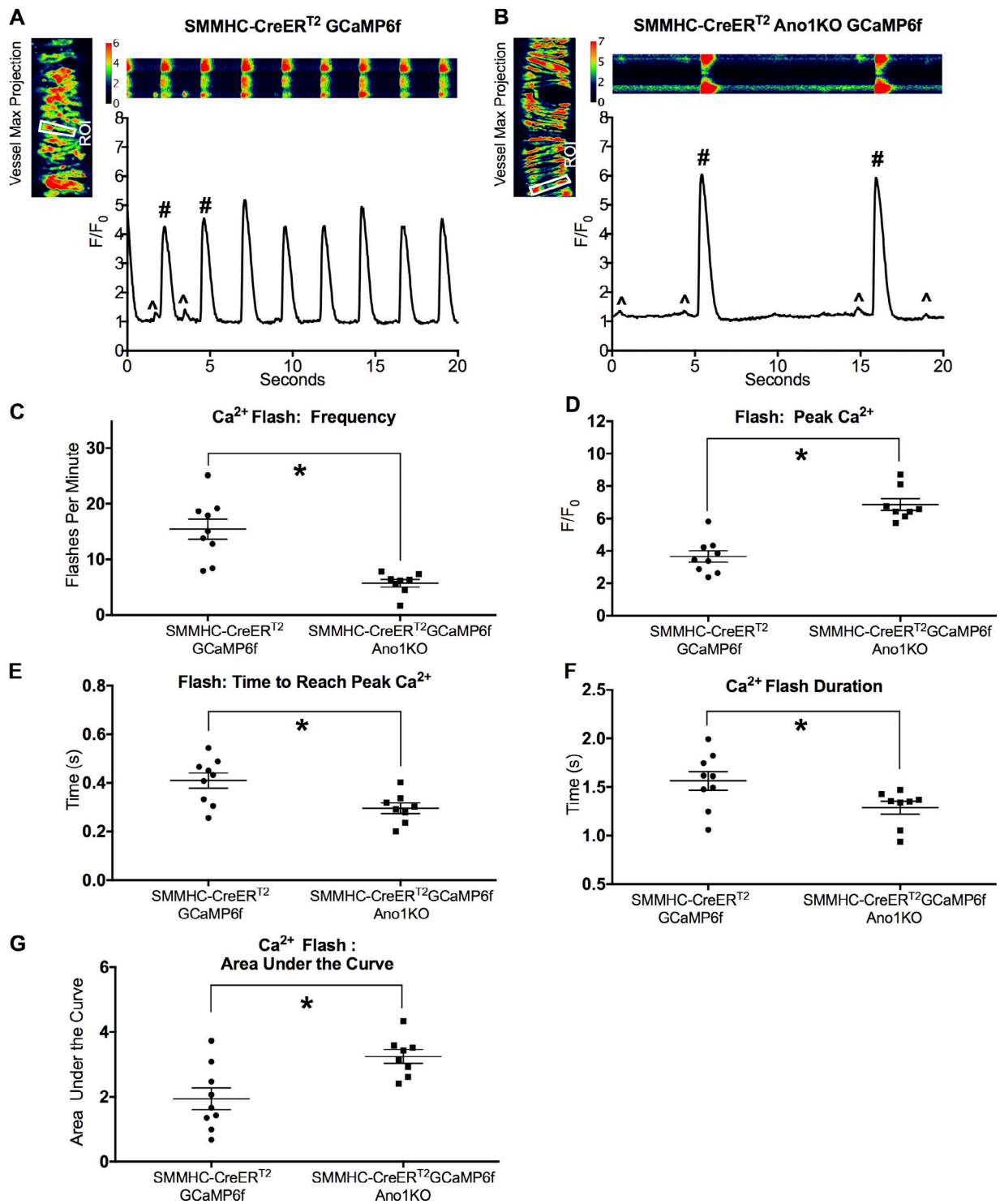


Figure 11. **Ca²⁺ flash analysis in pressurized IALV from SMMHC-CreER^{T2}-GCaMP6f-Ano1KO mice.** Pressurized (3 cm H₂O) control SMMHC-CreER^{T2}-GCaMP6f (A) and SMMHC-CreER^{T2}-GCaMP6f-Ano1KO (B) vessels were imaged at 20–33 fps with a 20× objective. Image sequences were made into maximum z-stack projections to create a single-cell mask to assess Ca²⁺ intensity over baseline (F/F₀). Ca²⁺ flashes (#) are indicative of action potential-generated Ca²⁺ influx through LTCCs, although spontaneous and local Ca²⁺ signals are also evident (*). Summary data for Ca²⁺ flash frequency (C), peak Ca²⁺ intensity (D), time to reach peak Ca²⁺ (E), Ca²⁺ flash duration (F), and the area under the curve (G) were measured. *, P < 0.05 comparing SMMHC-CreER^{T2}-Ano1KO versus Ano1fl/fl with n = 9 for control, n = 8 for SMMHC-CreER^{T2}-Ano1KO.

of these non-LMC Ano1⁺ adventitial cells and whether they form electrical junctions with LMCs is ongoing, but the fact that they did not form a contiguous network argues against their role as

pacemakers. The fact that LMCs express Ano1 and exhibit spontaneous calcium activity lends support to the hypothesis that LMCs act as their own intrinsic pacemaker.

Curiously, whole-cell Cl^- current recorded in LMCs demonstrated a slight inward rectification (Fig. 1). This contrasts with the majority of reports describing Anol/TMEM16A voltage sensitivity (Caputo et al., 2008; Schroeder et al., 2008; Yang et al., 2008) with outward rectification that linearizes with increasing Ca^{2+} (Caputo et al., 2008; Schroeder et al., 2008; Yang et al., 2008), although some others report an almost linear I-V relationship (Thomas-Gatewood et al., 2011; Burriss et al., 2015). Our “low” Ca^{2+} 200-nM patch pipette concentration would be sufficient to partially activate Anol but does not explain why we observed slight inward rectification that persisted at higher patch pipette Ca^{2+} concentrations. Differences in the I-V curves could also be attributed to different cell systems and internal/external buffer composition. We used the same solutions, NMDG bath, and CsCl in the pipette as in the studies reporting more linear I-V profiles (Thomas-Gatewood et al., 2011; Burriss et al., 2015). Additionally, we also performed our ramp protocol in the presence of nifedipine to rule out a potentially confounding voltage-gated L-type Ca^{2+} current. The Cl^- currents we recorded were impaired with the Anol inhibitor benzbramarone (Fig. 7 A), one of the more potent inhibitors currently available (Huang et al., 2012; Hwang et al., 2016), and were nearly absent in Anol^{smKO} LMCs generated using two different Anol^{fl/fl} lines and two different inducible smooth muscle-targeting Cre mice; thus, the shape of the I-V curve is unlikely to be strongly influenced by the presence of another Cl^- channel. Critically, the reversal potentials recorded when Cl^- was substituted with either glutamate or iodide matched the theoretical values expected for a pure Cl^- current, ruling down a major contaminating influence of other ions and channels (Fig. 1). Notably, CaCC currents recorded in patch-clamped LMCs from sheep mesenteric lymphatic vessels also demonstrated a significant inward Cl^- current at negative membrane potentials that was blocked with the nonselective I_{ClCa} inhibitor 9-AC (Toland et al., 2000). The disparity between the shape of the I-V curve for I_{ClCa} in LMCs and the I-V curve of Anol in vascular smooth muscle or heterologous expression systems could be due differences in the splice variant expressed (Ferrera et al., 2009; Sung et al., 2016), post-translational modifications to Anol, the surrounding membrane environment (Schreiber et al., 2018), or potential interactions with other proteins or channels, as documented for bestrophins (Dam et al., 2014a) and CFTR (Benedetto et al., 2017). Through its interaction with bestrophins, Anol has also been implicated as a component of the cGMP-sensitive Cl^- current (Dam et al., 2014a,b), although we found no evidence for a cGMP-sensitive Cl^- current in the LMCs in this study (Fig. 3, B–D). The lack of cGMP-sensitive Cl^- current in mouse LMCs is unsurprising given the evidence for Cl^- in the initiation of lymphatic contractile activity compared with the predominantly inhibitory role of cGMP/PKG signaling reported in LMCs (Gasheva et al., 2013; Mathias and von der Weid, 2013). Further investigations into the Anol splice variant expressed in lymphatic muscle and its possible interactions with other proteins within the LMC membrane are needed to resolve these issues.

The IALVs used for these studies have a relatively high baseline contractile frequency even at low pressures, in line with the findings of our recent study comparing the contractile

activity of lymphatic collecting vessels from multiple tissues (Zawieja et al., 2018). It is possible that regional differences in contractile frequency (Gashev et al., 2004; Zawieja et al., 2018) can be attributed to different Anol expression or activity. In arteries/arterioles, Anol has been linked to the myogenic response through its contribution to depolarizing the resting membrane potential and thereby increasing LTCC activity, resulting in vasoconstriction as pressure rises (Bulley et al., 2012). We observed a significant reduction in tone with benzbramarone, but in contrast, found no significant differences in tone between Anol^{ismKO} and Anol floxed control mice. In addition to its ability to inhibit Anol, benzbramarone has also been shown to act as an urate transporter inhibitor (Lee et al., 2008) and as an activator of voltage-gated KQT-like subfamily potassium (KCNQ) channels (Zheng et al., 2015). These and other unknown off-target actions could explain the potent tone inhibition and cessation of contractions, achieved at higher benzbramarone concentrations, as neither observation was recapitulated in the Anol^{smKO} IALVs even though the contraction frequency was almost identically reduced in both the Anol^{smKO} and benzbramarone-treated vessels. The hyperpolarizations we observed with 5 μM benzbramarone and in Anol^{smKO} IALVs were on the order of 4–6 mV, which may be insufficient to significantly alter lymphatic vessel tone. Additionally, or alternatively, there are likely to be contributing and potentially compensating actions of V_m -independent mechanisms that regulate vessel tone through the balancing actions of myosin light chain kinases and phosphatases shown to be involved in lymphatic vessel tone maintenance (Wang et al., 2009; Nepiyushchikh et al., 2011).

As recently documented (Zawieja et al., 2018), action potentials recorded in LMCs of pressurized murine IALVs are characterized by a slow, linear diastolic depolarization period that undergoes an exponential transformation upon reaching a critical voltage threshold to form the rapid upstroke of the action potential. A similar diastolic depolarization has been observed in rat and sheep vessels (Beckett et al., 2007; von der Weid et al., 2014) with a suggested role for I_{ClCa} . From our recordings, this slope is reduced nearly fourfold (from 7–8 mV/s to 2 mV/s) by deletion of Anol from the LMCs or by Anol inhibition with benzbramarone, suggesting a prominent role for Cl^- efflux in the determination of lymphatic pacemaking rate. Despite the significant reduction in contraction frequency and loss of pressure-dependent changes in contraction frequency, Anol does not appear to be obligatory for the initiation of the murine action potential, and other ion channels apparently contribute to the residual diastolic depolarization observed after Anol deletion. Other channels potentially involved in this basal diastolic depolarization could include voltage-gated sodium channels (Na_v) channels, hyperpolarization-activated cyclic nucleotide-gated (HCN) channels, Piezo channels, and potentially mechanosensitive transient receptor potential (TRP) channels (McCloskey et al., 1999; Lee et al., 2014; Telinius et al., 2015). In the pacemaking interstitial cells of Cajal located in the myenteric plexus, the depolarizing action of Anol is set by intracellular Cl^- , which accumulates through the action of NKCC1 (Zhu et al., 2016). The higher the intracellular concentration of Cl^- , the more positive the Cl^- equilibrium potential (E_{Cl}), which can

allow for a depolarizing current through Cl^- efflux from the cell. Smooth muscle cells are known to express NKCC1 (Wang et al., 2007), and we have observed expression of NKCC1 in purified LMCs from IALVs (Fig. 3 E), suggesting a similar axis is at play in the murine LMCs. This poses an interesting question as to whether the drugs furosemide and bumetanide, used as loop diuretics primarily through the inhibition of the NKCC2 isoform found in the kidney, but which also inhibit NKCC1, may inadvertently impair fluid removal out of the interstitial space through inhibition of LMC excitability. The roles of NKCC1 and LMC intracellular Cl^- concentration in the regulation of E_{Cl} in LMCs and their impact on the LMC diastolic depolarization warrant further examination.

The seminal work hypothesizing a role for I_{ClCa} was done in guinea pig mesenteric vessels, where spontaneous local Ca^{2+} events, termed puffs, were observed using fluorescent Ca^{2+} indicator dyes (Van Helden, 1993; von der Weid et al., 2008); these events were proposed to correlate with the spontaneous transient depolarizations observed in guinea pig mesenteric lymphatic vessels. The spontaneous transient depolarizations recorded in these preparations were sensitive to CaCC inhibitors, albeit inhibitors that do not distinguish well between cation and Cl^- channels (Van Helden, 1993; von der Weid et al., 2008). At a frame rate of 30 fps, we observed similar spontaneous Ca^{2+} signals (Fig. 11, ^ symbol) in the majority of LMCs in pressurized vessels expressing GCaMP6f in the LMC layer (Zawieja et al., 2018); however, we did not consistently detect spontaneous transient depolarizations in membrane recording preparations sampled at 1 kHz. These differences may be explained in part by the conditions under which spontaneous transient depolarizations are primarily observed: (1) single vessels cut into small pieces in an attempt to achieve isoelectric conditions, (2) unpressurized and unstretched vessels from (3) guinea pig mesentery, and (4) during or after LTCC inhibition (Van Helden, 1993; von der Weid et al., 2008). Given the high degree of electrical coordination among lymphatic LMCs (Castorena-Gonzalez et al., 2018; Hald et al., 2018), it is possible that the local inward Cl^- current generated in response to a Ca^{2+} event rapidly dissipates across the electrically coupled length of our isobaric preparation and that the diastolic depolarization rate we observed is the integration of spontaneous transient depolarizations interacting with other voltage-sensitive channels (Hald et al., 2018). Future studies combining both electrical and Ca^{2+} recordings in both single patch-clamped LMCs and whole vessels will be required to address these possibilities.

In addition to its role in action potential initiation, Anol1 activity makes a significant contribution to the duration and shape of the murine action potential, as the action potential plateau was absent in Anol1^{smKO} vessels. The murine IALV action potential often contains a brief 1–3-mV spike that approaches a potential of –5 mV before stabilizing at a sustained plateau potential around –11 to –10 mV (Zawieja et al., 2018). The presence of this relatively small spike, as opposed to the larger spike observed in rat and human lymphatics (von der Weid et al., 2014; Telinius et al., 2015), could be due to differences in voltage-gated sodium channel expression. In control IALVs, the duration of the LMC action potential plateau is significantly

elongated by the L-type channel agonist BayK8644 (Zawieja et al., 2018), while inhibition of L-type channels with nifedipine abolishes action potentials, leading to a static resting membrane potential (von der Weid et al., 2008). In contrast, Anol1^{smKO} action potentials had peak potentials around +15 to +20 mV, lacked the plateau phase, and were shorter in duration, quickly repolarizing to a lower resting membrane potential than observed in controls (Fig. 9). We conclude from these findings that (1) Anol1 provides a baseline depolarizing current that contributes to resting membrane potential and diastolic depolarization; (2) upon reaching threshold, LTCCs open, resulting in an influx of Ca^{2+} that directly or indirectly (through Ca^{2+} -induced Ca^{2+} release) activates Anol1; (3) the transition of the action potential spike into a plateau can be explained by the initial electrogenic Ca^{2+} influx from voltage-gated Ca^{2+} channels that quickly resolves into the plateau potential centered on E_{Cl} as Anol1 remains activated; and (4) action potential plateau duration is set by the combined action of Anol1 and LTCCs. These conclusions are further supported by the fact that the action potential exponential depolarization was steeper (a lower upstroke rate constant τ , Fig. 9) and the time to reach the peak Ca^{2+} flash was shorter in Anol1^{smKO} IALVs. The peak of the action potential was more positive and Ca^{2+} flash intensity was higher in Anol1^{smKO} IALVs, and both action potential duration and Ca^{2+} flash duration were shorter in the Anol1^{smKO} IALVs. The diffuse staining of Anol1 within the LMCs, as opposed to just localized puncta, further supports our interpretation that both local Ca^{2+} signals from the SR during the initiation of the action potential, and its associated global Ca^{2+} flash, can activate Anol1 channels. Additionally, the contribution of Ca^{2+} activated K^+ channels (K_{Ca}) and voltage-gated K^+ channels (K_{v}) channels to the murine lymphatic action potential are currently unknown and could be differentially involved in Anol1^{smKO} IALVs due to the altered Ca^{2+} and voltage dynamics. Additional studies using more selective pharmaceutical agents and/or KO mice are required to further understand and model the ionic components of the murine lymphatic action potential.

Lastly, despite the significant increase in peak Ca^{2+} and peak Ca^{2+} rise time, we did not observe any consistent or significant effect on contraction amplitude with Anol1 inhibition or in Anol1^{smKO} IALVs. In our recent report (Zawieja et al., 2018), we demonstrated that the IALV contraction frequency was significantly reduced and contraction amplitude significantly increased with the LTCC agonist BayK8644. In that study, contraction frequency was reduced, not as a result of changes to the diastolic depolarization rate or the diastolic period, but due to a doubling in the duration of the action potential plateau phase (Zawieja et al., 2018). It also is worth noting that plateau potential remained unchanged after BayK8644 stimulation (Zawieja et al., 2018), providing further evidence that the murine lymphatic action potential is dominated by Cl^- . While the contraction amplitude in WT IALVs increased with BayK8644, BayK8644 increased both the peak Ca^{2+} signal intensity and duration (Zawieja et al., 2018); in contrast, Anol1^{smKO} IALVs had a significantly reduced Ca^{2+} flash duration, and the increase in peak flash Ca^{2+} was not as large as achieved with BayK8644-treated control vessels in our previous study (Zawieja et al., 2018).

To circumvent the lethality associated with the *Ano1*^{-/-}-null mice and to specifically target the lymphatic muscle cells, we used SMMHC-CreER^{T2} and SMAR^TTa-tetOCre lines that allowed us to direct the recombination to smooth muscle cells. This enabled us to specifically address the role of *Ano1* in lymphatic muscle cells within our isolated vessel preparation. Despite the advantages offered by the inducible Cre mice, they are nonetheless limited by their induction and recombination efficiency and fidelity of the promoter in recapitulating the specific expression. We were unable to achieve 100% recombination in all LMCs with either of our inducible Cre lines SMMHC-CreER^{T2} and SMAR^TTa-tetOCre, based on our ROSA26mT/mG reporter. Furthermore, it is possible that Cre-directed recombination of ROSA26mT/mG does not equate to successful recombination of both *Ano1* alleles in the *Ano1*^{smKO} mice. We attempted to use the constitutive smMHC^{Cre/eGFP} line to overcome the potential shortcomings of the induction efficiency inherent to inducible Cre models. Unfortunately, the smMHC^{Cre/eGFP} transgene was not visible in all LMCs, and the GFP⁺ LMCs were quite variable in their fluorescence intensity, implying a similar variability in Cre expression and recombination efficiency. We attribute the slightly higher average contraction frequency seen in the smMHC^{Cre/eGFP}-*Ano1*KO IALVs to lower penetrance of the smMHC^{Cre/eGFP} within the lymphatic muscle layer, limiting the usefulness of this Cre line in future lymphatic studies. We have also yet to see any gross manifestations of lymphedema within the mouse limbs in smMHC^{Cre/eGFP}-*Ano1*^{smKO} mice within our colony up to 1 yr despite the reduction in contraction frequency. However, the manifestation of lymphedema due to lymphatic contractile dysfunction in mice may require a chronic gravitational load (Castorena-Gonzalez et al., 2018). Deletion of *Ano1* has been shown to reduce the expression of LTCCs in vascular smooth muscle (Dam et al., 2014b); however, we did not observe any significant impairment in contraction amplitude, which is sensitive to LTCC inhibition. It is possible that a reduction in contraction amplitude due to a reduction in L-type calcium channels could be observed at a later time point.

Conclusions

Ano1 is functionally expressed in LMCs and accounts for the majority, if not the totality, of the *I*_{ClCa} in LMCs. *Ano1*-mediated Cl⁻ current is critical for pressure-dependent modulation of contraction frequency of murine lymphatic vessels through its role in setting the resting membrane potential and diastolic depolarization rate, but *Ano1* deletion from LMCs does not eliminate spontaneous contractions. *Ano1* is likely activated in response to both spontaneous Ca²⁺ release from the SR and Ca²⁺ influx through LTCCs in mouse lymphatic muscle. Further investigations into the pressure-dependent mechanism of *Ano1* activation during diastole are warranted.

Acknowledgments

The authors would like to thank Sean Ward for his advice in the preparation and collection of sharp electrode intracellular membrane potential measurements. We would also like to thank Stefan Offermanns, Max-Planck-Intstitut für Herz- und

Lungendforschung, Bad Nauheim, Germany, for donation of the SMMHC-CreER^{T2} mice, and Dieter Saur, Technical University of Munich, Munich, Germany, for his donation of c-KitCreER^{T2} mice. Finally, we would like to thank Grant Hennig and Bernard T. Drumm for their technical guidance in our analysis of the LMC calcium recordings.

This work was supported by National Heart, Lung, and Blood Institute-National Institutes of Health grants R01 HL122578 and R01 HL125608 to M.J. Davis, and R01 HL133256 and HL137745 to J.H. Jaggar, and an American Heart Association Scientist Development Grant 16SDG27460007 to S.A. Bulley.

The authors declare no competing financial interests.

Author contributions: S.D. Zawieja and M.J. Davis conceived and designed the experiments. J.R. Rock provided *Ano1*^{f^{fl}R/f^{fl}R} and SMAR^TTa-tetOCre mice. J.H. Jaggar and S.A. Bulley provided the *Ano1*^{f^{fl}/f^{fl}} mice and SMMHC-CreER^{T2}. S.D. Zawieja, J.A. Castorena, P. Gui, and M. Li performed the studies, and collected and analyzed the data. S.D. Zawieja, J.A. Castorena, S.A. Bulley, J. R. Rock, J.H. Jaggar, and M.J. Davis interpreted the data, drafted the manuscript, and revised it critically for intellectual concepts and content. All authors have approved the final draft of the manuscript, and their contributions qualify them as authors.

Merritt C. Maduke served as editor.

Submitted: 20 November 2018

Accepted: 6 February 2019

References

- Beckett, E.A., M.A. Hollywood, K.D. Thornbury, and N.G. McHale. 2007. Spontaneous electrical activity in sheep mesenteric lymphatics. *Lymphat. Res. Biol.* 5:29–43. <https://doi.org/10.1089/lrb.2007.5104>
- Benedetto, R., J. Ousingsawat, P. Wanitchakool, Y. Zhang, M.J. Holtzman, M. Amaral, J.R. Rock, R. Schreiber, and K. Kunzelmann. 2017. Epithelial Chloride Transport by CFTR Requires TMEM16A. *Sci. Rep.* 7:12397. <https://doi.org/10.1038/s41598-017-10910-0>
- Briggs Boedtker, D., J. Rumessen, U. Baandrup, M. Skov Mikkelsen, N. Tellingius, H. Pilegaard, C. Aalkjaer, and V. Hjordal. 2013. Identification of interstitial Cajal-like cells in the human thoracic duct. *Cells Tissues Organs.* 197:145–158. <https://doi.org/10.1159/000342437>
- Bulley, S., Z.P. Neeb, S.K. Burris, J.P. Bannister, C.M. Thomas-Gatewood, W. Jangsangthong, and J.H. Jaggar. 2012. TMEM16A/ANO1 channels contribute to the myogenic response in cerebral arteries. *Circ. Res.* 111:1027–1036. <https://doi.org/10.1161/CIRCRESAHA.112.277145>
- Burris, S.K., Q. Wang, S. Bulley, Z.P. Neeb, and J.H. Jaggar. 2015. 9-Phenanthroline inhibits recombinant and arterial myocyte TMEM16A channels. *Br. J. Pharmacol.* 172:2459–2468. <https://doi.org/10.1111/bph.13077>
- Caputo, A., E. Caci, L. Ferrera, N. Pedemonte, C. Barsanti, E. Sondo, U. Pfeiffer, R. Ravazzolo, O. Zegarra-Moran, and L.J. Galiotta. 2008. TMEM16A, a membrane protein associated with calcium-dependent chloride channel activity. *Science.* 322:590–594. <https://doi.org/10.1126/science.1163518>
- Castorena-Gonzalez, J.A., S.D. Zawieja, M. Li, R.S. Srinivasan, A.M. Simon, C. de Wit, R. de la Torre, L.A. Martinez-Lemus, G.W. Hennig, and M.J. Davis. 2018. Mechanisms of Connexin-Related Lymphedema. *Circ. Res.* 123:964–985. <https://doi.org/10.1161/CIRCRESAHA.117.312576>
- Chatterjee, V., and A.A. Gashev. 2012. Aging-associated shifts in functional status of mast cells located by adult and aged mesenteric lymphatic vessels. *Am. J. Physiol. Heart Circ. Physiol.* 303:H693–H702. <https://doi.org/10.1152/ajpheart.00378.2012>
- Chen, T.W., T.J. Wardill, Y. Sun, S.R. Pulver, S.L. Renninger, A. Baohan, E.R. Schreiter, R.A. Kerr, M.B. Orger, V. Jayaraman, et al. 2013. Ultrasensitive fluorescent proteins for imaging neuronal activity. *Nature.* 499:295–300. <https://doi.org/10.1038/nature12354>
- Dam, V.S., D.M. Boedtker, C. Aalkjaer, and V. Matchkov. 2014a. The bestrophin- and TMEM16A-associated Ca(2+)-activated Cl(-) channels in

- vascular smooth muscles. *Channels (Austin)*. 8:361–369. <https://doi.org/10.4161/chan.29531>
- Dam, V.S., D.M. Boedtker, J. Nyvad, C. Aalkjaer, and V. Matchkov. 2014b. TMEM16A knockdown abrogates two different Ca(2+)-activated Cl (-) currents and contractility of smooth muscle in rat mesenteric small arteries. *Pflugers Arch*. 466:1391–1409. <https://doi.org/10.1007/s00424-013-1382-1>
- Davis, M.J., M.M. Lane, A.M. Davis, D. Durtschi, D.C. Zawieja, M. Muthuchamy, and A.A. Gashev. 2008. Modulation of lymphatic muscle contractility by the neuropeptide substance P. *Am. J. Physiol. Heart Circ. Physiol.* 295:H587–H597. <https://doi.org/10.1152/ajpheart.01029.2007>
- Davis, M.J., A.M. Davis, C.W. Ku, and A.A. Gashev. 2009. Myogenic constriction and dilation of isolated lymphatic vessels. *Am. J. Physiol. Heart Circ. Physiol.* 296:H293–H302. <https://doi.org/10.1152/ajpheart.01040.2008>
- Davis, M.J., E. Rahbar, A.A. Gashev, D.C. Zawieja, and J.E. Moore Jr. 2011. Determinants of valve gating in collecting lymphatic vessels from rat mesentery. *Am. J. Physiol. Heart Circ. Physiol.* 301:H48–H60. <https://doi.org/10.1152/ajpheart.00133.2011>
- Davis, M.J., J.P. Scallan, J.H. Wolpers, M. Muthuchamy, A.A. Gashev, and D.C. Zawieja. 2012. Intrinsic increase in lymphangion muscle contractility in response to elevated afterload. *Am. J. Physiol. Heart Circ. Physiol.* 303:H795–H808. <https://doi.org/10.1152/ajpheart.01097.2011>
- Drumm, B.T., G.W. Hennig, M.J. Battersby, E.K. Cunningham, T.S. Sung, S.M. Ward, K.M. Sanders, and S.A. Baker. 2017. Clustering of Ca²⁺ transients in interstitial cells of Cajal defines slow wave duration. *J. Gen. Physiol.* 149:703–725. <https://doi.org/10.1085/jgp.201711771>
- Duffy, A.M., C.A. Cobine, and K.D. Keef. 2012. Changes in neuromuscular transmission in the W/W^v mouse internal anal sphincter. *Neurogastroenterol. Motil.* 24:e41–e55. <https://doi.org/10.1111/j.1365-2982.2011.01806.x>
- Ferrera, L., A. Caputo, I. Ubbay, E. Bussani, O. Zegarra-Moran, R. Ravazzolo, F. Pagani, and L.J. Galietta. 2009. Regulation of TMEM16A chloride channel properties by alternative splicing. *J. Biol. Chem.* 284:33360–33368. <https://doi.org/10.1074/jbc.M109.046607>
- Furuya, M., S.B. Kirschbaum, A. Paulovich, B.U. Pauli, H. Zhang, J.S. Alexander, A.G. Farr, and A. Ruddell. 2010. Lymphatic endothelial murine chloride channel calcium-activated 1 is a ligand for leukocyte LFA-1 and Mac-1. *J. Immunol.* 185:5769–5777. <https://doi.org/10.4049/jimmunol.1002226>
- Gashev, A.A., M.J. Davis, M.D. Delp, and D.C. Zawieja. 2004. Regional variations of contractile activity in isolated rat lymphatics. *Microcirculation*. 11:477–492. <https://doi.org/10.1080/10739680490476033>
- Gasheva, O.Y., A.A. Gashev, and D.C. Zawieja. 2013. Cyclic guanosine monophosphate and the dependent protein kinase regulate lymphatic contractility in rat thoracic duct. *J. Physiol.* 591:4549–4565. <https://doi.org/10.1113/jphysiol.2013.258681>
- Gomez-Pinilla, P.J., S.J. Gibbons, M.R. Bardsley, A. Lorincz, M.J. Pozo, P.J. Pasricha, M. Van de Rijn, R.B. West, M.G. Sarr, M.L. Kendrick, et al. 2009. Anol1 is a selective marker of interstitial cells of Cajal in the human and mouse gastrointestinal tract. *Am. J. Physiol. Gastrointest. Liver Physiol.* 296:G1370–G1381. <https://doi.org/10.1152/ajpgi.00074.2009>
- Hald, B.O., J.A. Castorena-Gonzalez, S.D. Zawieja, P. Gui, and M.J. Davis. 2018. Electrical Communication in Lymphangions. *Biophys. J.* 115:936–949. <https://doi.org/10.1016/j.bpj.2018.07.033>
- Hasselhof, V., A. Sperling, K. Buttler, P. Ströbel, J. Becker, T. Aung, G. Felmerer, and J. Wilting. 2016. Morphological and Molecular Characterization of Human Dermal Lymphatic Collectors. *PLoS One*. 11:e0164964. <https://doi.org/10.1371/journal.pone.0164964>
- He, M., W. Ye, W.J. Wang, E.S. Sison, Y.N. Jan, and L.Y. Jan. 2017. Cytoplasmic Cl⁻ couples membrane remodeling to epithelial morphogenesis. *Proc. Natl. Acad. Sci. USA*. 114:E11161–E11169. <https://doi.org/10.1073/pnas.1714448115>
- Heger, K., B. Seidler, J.C. Vahl, C. Schwartz, M. Kober, S. Klein, D. Voehringer, D. Saur, and M. Schmidt-Supprian. 2014. CreER(T2) expression from within the c-Kit gene locus allows efficient inducible gene targeting in and ablation of mast cells. *Eur. J. Immunol.* 44:296–306. <https://doi.org/10.1002/eji.201343731>
- Hennig, G.W., N.J. Spencer, S. Jokela-Willis, P.O. Bayguinov, H.T. Lee, L.A. Ritchie, S.M. Ward, T.K. Smith, and K.M. Sanders. 2010. ICC-MY coordinate smooth muscle electrical and mechanical activity in the murine small intestine. *Neurogastroenterol. Motil.* 22:e138–e151.
- Hollywood, M.A., K.D. Cotton, K.D. Thornbury, and N.G. McHale. 1997. Tetrodotoxin-sensitive sodium current in sheep lymphatic smooth muscle. *J. Physiol.* 503:13–20. <https://doi.org/10.1111/j.1469-7793.1997.013bi.x>
- Huang, F., H. Zhang, M. Wu, H. Yang, M. Kudo, C.J. Peters, P.G. Woodruff, O. D. Solberg, M.L. Donne, X. Huang, et al. 2012. Calcium-activated chloride channel TMEM16A modulates mucin secretion and airway smooth muscle contraction. *Proc. Natl. Acad. Sci. USA*. 109:16354–16359. <https://doi.org/10.1073/pnas.1214596109>
- Hwang, S.J., P.J. Blair, F.C. Britton, K.E. O'Driscoll, G. Hennig, Y.R. Bayguinov, J.R. Rock, B.D. Harfe, K.M. Sanders, and S.M. Ward. 2009. Expression of anoctamin 1/TMEM16A by interstitial cells of Cajal is fundamental for slow wave activity in gastrointestinal muscles. *J. Physiol.* 587:4887–4904. <https://doi.org/10.1113/jphysiol.2009.176198>
- Hwang, S.J., N. Basma, K.M. Sanders, and S.M. Ward. 2016. Effects of new-generation inhibitors of the calcium-activated chloride channel anoctamin 1 on slow waves in the gastrointestinal tract. *Br. J. Pharmacol.* 173:1339–1349. <https://doi.org/10.1111/bph.13431>
- Lee, M.H., G.G. Graham, K.M. Williams, and S.O. Day. 2008. A benefit-risk assessment of benzbromarone in the treatment of gout. Was its withdrawal from the market in the best interest of patients? *Drug Saf.* 31:643–665. <https://doi.org/10.2165/0002018-200831080-00002>
- Lee, S., S. Roizes, and P.Y. von der Weid. 2014. Distinct roles of L- and T-type voltage-dependent Ca²⁺ channels in regulation of lymphatic vessel contractile activity. *J. Physiol.* 592:5409–5427. <https://doi.org/10.1113/jphysiol.2014.280347>
- Malysz, J., S.J. Gibbons, S.A. Saravanaperumal, P. Du, S.T. Eisenman, C. Cao, U. Oh, D. Saur, S. Klein, T. Ordog, and G. Farrugia. 2017. Conditional genetic deletion of Anol1 in interstitial cells of Cajal impairs Ca²⁺ transients and slow waves in adult mouse small intestine. *Am. J. Physiol. Gastrointest. Liver Physiol.* 312:G228–G245. <https://doi.org/10.1152/ajpgi.00363.2016>
- Mathias, R., and P.Y. von der Weid. 2013. Involvement of the NO-cGMP-K (ATP) channel pathway in the mesenteric lymphatic pump dysfunction observed in the guinea pig model of TNBS-induced ileitis. *Am. J. Physiol. Gastrointest. Liver Physiol.* 304:G623–G634. <https://doi.org/10.1152/ajpgi.00392.2012>
- McCloskey, K.D., H.M. Toland, M.A. Hollywood, K.D. Thornbury, and N.G. McHale. 1999. Hyperpolarisation-activated inward current in isolated sheep mesenteric lymphatic smooth muscle. *J. Physiol.* 521:201–211. <https://doi.org/10.1111/j.1469-7793.1999.00201.x>
- McCloskey, K.D., M.A. Hollywood, K.D. Thornbury, S.M. Ward, and N.G. McHale. 2002. Kit-like immunopositive cells in sheep mesenteric lymphatic vessels. *Cell Tissue Res.* 310:77–84. <https://doi.org/10.1007/s00441-002-0623-y>
- Mohanakumar, S., J. Majgaard, N. Telinius, N. Katballe, E. Pahle, V. Hjorddal, and D. Boedtker. 2018. Spontaneous and α -adrenoceptor-induced contractility in human collecting lymphatic vessels require chloride. *Am. J. Physiol. Heart Circ. Physiol.* 315:H389–H401. <https://doi.org/10.1152/ajpheart.00551.2017>
- Muzumdar, M.D., B. Tasic, K. Miyamichi, L. Li, and L. Luo. 2007. A global double-fluorescent Cre reporter mouse. *Genesis*. 45:593–605. <https://doi.org/10.1002/dvg.20335>
- Nepiyushchikh, Z.V., S. Chakraborty, W. Wang, M.J. Davis, D.C. Zawieja, and M. Muthuchamy. 2011. Differential effects of myosin light chain kinase inhibition on contractility, force development and myosin light chain 20 phosphorylation of rat cervical and thoracic duct lymphatics. *J. Physiol.* 589:5415–5429. <https://doi.org/10.1113/jphysiol.2011.218446>
- Olszewski, W.L. 2002. Contractility patterns of normal and pathologically changed human lymphatics. *Ann. N. Y. Acad. Sci.* 979:52–63. <https://doi.org/10.1111/j.1749-6632.2002.tb04867.x>
- Sala-Rabanal, M., Z. Yurtsever, C.G. Nichols, and T.J. Brett. 2015. Secreted CLCA1 modulates TMEM16A to activate Ca(2+)-dependent chloride currents in human cells. *eLife*. 4:e05875. <https://doi.org/10.7554/eLife.05875>
- Scallan, J.P., and M.J. Davis. 2013. Genetic removal of basal nitric oxide enhances contractile activity in isolated murine collecting lymphatic vessels. *J. Physiol.* 591:2139–2156. <https://doi.org/10.1113/jphysiol.2012.250662>
- Schreiber, R., D. Faria, B.V. Skryabin, P. Wanitchakool, J.R. Rock, and K. Kunzelmann. 2015. Anoctamins support calcium-dependent chloride secretion by facilitating calcium signaling in adult mouse intestine. *Pflugers Arch*. 467:1203–1213. <https://doi.org/10.1007/s00424-014-1559-2>
- Schreiber, R., J. Ousingawat, P. Wanitchakool, L. Sirianant, R. Benedetto, K. Reiss, and K. Kunzelmann. 2018. Regulation of TMEM16A/ANO1 and TMEM16F/ANO6 ion currents and phospholipid scrambling by Ca²⁺ and

- plasma membrane lipid. *J. Physiol.* 596:217–229. <https://doi.org/10.1113/JP275175>
- Schroeder, B.C., T. Cheng, Y.N. Jan, and L.Y. Jan. 2008. Expression cloning of TMEM16A as a calcium-activated chloride channel subunit. *Cell*. 134: 1019–1029. <https://doi.org/10.1016/j.cell.2008.09.003>
- Scudieri, P., E. Sondo, L. Ferrera, and L.J. Galletta. 2012. The anoctamin family: TMEM16A and TMEM16B as calcium-activated chloride channels. *Exp. Physiol.* 97:177–183. <https://doi.org/10.1113/expphysiol.2011.058198>
- Sung, T.S., K. O'Driscoll, H. Zheng, N.J. Yapp, N. Leblanc, S.D. Koh, and K.M. Sanders. 2016. Influence of intracellular Ca²⁺ and alternative splicing on the pharmacological profile of ANO1 channels. *Am. J. Physiol. Cell Physiol.* 311:C437–C451. <https://doi.org/10.1152/ajpcell.00070.2016>
- Telinus, N., J. Majgaard, S. Kim, N. Katballe, E. Pahle, J. Nielsen, V. Hjortdal, C. Aalkjaer, and D.B. Boedtker. 2015. Voltage-gated sodium channels contribute to action potentials and spontaneous contractility in isolated human lymphatic vessels. *J. Physiol.* 593:3109–3122. <https://doi.org/10.1113/JP270166>
- Thomas-Gatewood, C., Z.P. Neeb, S. Bulley, A. Adebisi, J.P. Bannister, M.D. Leo, and J.H. Jagger. 2011. TMEM16A channels generate Ca²⁺-activated Cl⁻ currents in cerebral artery smooth muscle cells. *Am. J. Physiol. Heart Circ. Physiol.* 301:H1819–H1827. <https://doi.org/10.1152/ajpheart.00404.2011>
- Toland, H.M., K.D. McCloskey, K.D. Thornbury, N.G. McHale, and M.A. Hollywood. 2000. Ca(2+)-activated Cl(-) current in sheep lymphatic smooth muscle. *Am. J. Physiol. Cell Physiol.* 279:C1327–C1335. <https://doi.org/10.1152/ajpcell.2000.279.5.C1327>
- Torihashi, S., S.M. Ward, S. Nishikawa, K. Nishi, S. Kobayashi, and K.M. Sanders. 1995. c-kit-dependent development of interstitial cells and electrical activity in the murine gastrointestinal tract. *Cell Tissue Res.* 280:97–111.
- Truett, G.E., P. Heeger, R.L. Mynatt, A.A. Truett, J.A. Walker, and M.L. Warman. 2000. Preparation of PCR-quality mouse genomic DNA with hot sodium hydroxide and tris (HotSHOT). *Biotechniques.* 29:52–54. <https://doi.org/10.2144/00291bm09>
- Van Helden, D.F. 1993. Pacemaker potentials in lymphatic smooth muscle of the guinea-pig mesentery. *J. Physiol.* 471:465–479. <https://doi.org/10.1113/jphysiol.1993.sp019910>
- von der Weid, P.Y., J. Zhao, and D.F. Van Helden. 2001. Nitric oxide decreases pacemaker activity in lymphatic vessels of guinea pig mesentery. *Am. J. Physiol. Heart Circ. Physiol.* 280:H2707–H2716. <https://doi.org/10.1152/ajpheart.2001.280.6.H2707>
- von der Weid, P.Y., M. Rahman, M.S. Imtiaz, and D.F. van Helden. 2008. Spontaneous transient depolarizations in lymphatic vessels of the guinea pig mesentery: pharmacology and implication for spontaneous contractility. *Am. J. Physiol. Heart Circ. Physiol.* 295:H1989–H2000. <https://doi.org/10.1152/ajpheart.00007.2008>
- von der Weid, P.Y., S. Lee, M.S. Imtiaz, D.C. Zawieja, and M.J. Davis. 2014. Electrophysiological properties of rat mesenteric lymphatic vessels and their regulation by stretch. *Lymphat. Res. Biol.* 12:66–75. <https://doi.org/10.1089/lrb.2013.0045>
- Wang, W., Z. Nepiyushchikh, D.C. Zawieja, S. Chakraborty, S.D. Zawieja, A.A. Gashev, M.J. Davis, and M. Muthuchamy. 2009. Inhibition of myosin light chain phosphorylation decreases rat mesenteric lymphatic contractile activity. *Am. J. Physiol. Heart Circ. Physiol.* 297:H726–H734. <https://doi.org/10.1152/ajpheart.00312.2009>
- Wang, X., J. Breaks, K. Loutzenhiser, and R. Loutzenhiser. 2007. Effects of inhibition of the Na⁺/K⁺/2Cl⁻ cotransporter on myogenic and angiotensin II responses of the rat afferent arteriole. *Am. J. Physiol. Renal Physiol.* 292:F999–F1006. <https://doi.org/10.1152/ajprenal.00343.2006>
- Wirth, A., Z. Benyó, M. Lukasova, B. Leutgeb, N. Wettschureck, S. Gorbey, P. Orsy, B. Horváth, C. Maser-Gluth, E. Greiner, et al. 2008. G12-G13-LARG-mediated signaling in vascular smooth muscle is required for salt-induced hypertension. *Nat. Med.* 14:64–68. <https://doi.org/10.1038/nm1666>
- Xin, H.B., K.Y. Deng, M. Rishniw, G. Ji, and M.I. Kotlikoff. 2002. Smooth muscle expression of Cre recombinase and eGFP in transgenic mice. *Physiol. Genomics.* 10:211–215. <https://doi.org/10.1152/physiolgenomics.00054.2002>
- Yang, Y.D., H. Cho, J.Y. Koo, M.H. Tak, Y. Cho, W.S. Shim, S.P. Park, J. Lee, B. Lee, B.M. Kim, et al. 2008. TMEM16A confers receptor-activated calcium-dependent chloride conductance. *Nature.* 455:1210–1215. <https://doi.org/10.1038/nature07313>
- Zawieja, D.C. 2009. Contractile physiology of lymphatics. *Lymphat. Res. Biol.* 7:87–96. <https://doi.org/10.1089/lrb.2009.0007>
- Zawieja, S.D., J.A. Castorena-Gonzalez, B. Dixon, and M.J. Davis. 2017. Experimental Models Used to Assess Lymphatic Contractile Function. *Lymphat. Res. Biol.* 15:331–342. <https://doi.org/10.1089/lrb.2017.0052>
- Zawieja, S.D., J.A. Castorena-Gonzalez, J.P. Scallan, and M.J. Davis. 2018. Differences in L-type Ca²⁺ channel activity partially underlie the regional dichotomy in pumping behavior by murine peripheral and visceral lymphatic vessels. *Am. J. Physiol. Heart Circ. Physiol.* 314: H991–H1010. <https://doi.org/10.1152/ajpheart.00499.2017>
- Zhang, R., A.I. Taucer, A.A. Gashev, M. Muthuchamy, D.C. Zawieja, and M.J. Davis. 2013. Maximum shortening velocity of lymphatic muscle approaches that of striated muscle. *Am. J. Physiol. Heart Circ. Physiol.* 305: H1494–H1507. <https://doi.org/10.1152/ajpheart.00898.2012>
- Zheng, Y., H. Xu, L. Zhan, X. Zhou, X. Chen, and Z. Gao. 2015. Activation of peripheral KCNQ channels relieves gout pain. *Pain.* 156:1025–1035.
- Zhu, M.H., T.S. Sung, M. Kurahashi, L.E. O'Kane, K. O'Driscoll, S.D. Koh, and K.M. Sanders. 2016. Na⁺-K⁺-Cl⁻ cotransporter (NKCC) maintains the chloride gradient to sustain pacemaker activity in interstitial cells of Cajal. *Am. J. Physiol. Gastrointest. Liver Physiol.* 311:G1037–G1046. <https://doi.org/10.1152/ajpgi.00277.2016>